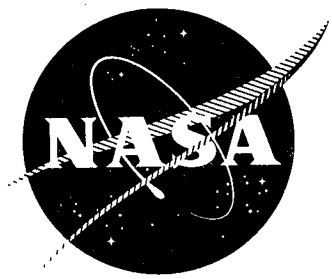

NASA CR-54589
GE R68AEG318

EXPERIMENTAL EVALUATION OF OUTER CASE BLOWING OR BLEEDING OF SINGLE STAGE AXIAL FLOW COMPRESSOR

PART III - PERFORMANCE OF BLOWING INSERT CONFIGURATION NO. 1

by

C.C. KOCH and L.H. SMITH, JR.

prepared for

NATIONAL AERONAUTICS AND SPACE ADMINISTRATION

CONTRACT NAS 3-7618

AIRCRAFT ENGINE TECHNICAL DIVISION
AIRCRAFT ENGINE GROUP
GENERAL ELECTRIC
LYNN, MASSACHUSETTS/CINCINNATI, OHIO

NASA CR-54589
GE R68AEG318

EXPERIMENTAL EVALUATION OF OUTER CASE BLOWING OR BLEEDING OF SINGLE STAGE AXIAL FLOW COMPRESSOR PART III - PERFORMANCE OF BLOWING INSERT CONFIGURATION NO. 1

by

C. C. Koch and L. H. Smith, Jr.

prepared for

NATIONAL AERONAUTICS AND SPACE ADMINISTRATION

November 22, 1968

CONTRACT NO. NAS3-7618

Technical Management
NASA Lewis Research Center
Cleveland, Ohio

James J. Watt, Project Manager
Everett E. Bailey, Research Advisor

AIRCRAFT ENGINE TECHNICAL DIVISION
AIRCRAFT ENGINE GROUP
GENERAL ELECTRIC COMPANY
WEST LYNN, MASSACHUSETTS/CINCINNATI, OHIO

EXPERIMENTAL EVALUATION OF OUTER CASE BLOWING OR BLEEDING OF SINGLE STAGE AXIAL FLOW COMPRESSOR

PART III - PERFORMANCE OF BLOWING INSERT CONFIGURATION NO. 1

by

C. C. Koch and L. H. Smith, Jr.

ABSTRACT

So that air could be injected at the tip for boundary layer control, a 1120 feet per second tip speed rotor having an aspect ratio of 4.5 and an inlet hub-tip radius ratio of 0.5 was equipped with a perforated outer casing. Testing was conducted with distorted as well as undistorted inlet flow, and overall and stalling performance were obtained for each inlet condition. For distorted inlet flow, rotating stalls began at the tip of the rotor, and the injection of boundary layer control air was effective in increasing stall margin. With undistorted inlet flow, rotating stall began at the pitchline for this rotor, and tip blowing did not produce significant improvements in stall margin.

SUMMARY

The objective of this program is to investigate the potential of outer casing blowing and bleeding as means of increasing the weight flow range of a 1120 feet per second tip speed rotor which has an aspect ratio of 4.5, an inlet hub-tip radius ratio of 0.5 and a design tip diffusion factor of 0.45. This report documents the performance of the rotor when equipped with an outer casing blowing device located above the rotor tip.

Tests were conducted with undistorted inlet flow and also with an inlet casing boundary layer trip, radial inlet distortion and circumferential distortion. Overall performance and stall performance were determined both with and without blowing flow.

Stall margin with undistorted inlet flow and with the boundary layer trip installed was not significantly improved by the tip blowing because the rotating stall cells initiated in the pitchline region. With zero blowing flow supplied, however, the prescence of the perforated casing over the rotor tip had a small beneficial effect on stall margin relative to previous plain casing test results.

With both inlet flow distortions, the rotating stall cells initiated at the tip, and the application of tip blowing was effective in increasing stall margin. With zero blowing air supplied, the radial inlet distortion stall line was reduced considerably below the undistorted inlet results. The circumferential inlet distortion stall line with zero blowing flow indicated larger stall margins than for the undistorted inlet condition with zero blowing flow. Although the stalling pressure ratio decreased with the circumferential distortion present, this was more than offset by a large decrease in stalling weight flow. Full understanding of this unexpected result will require further testing with more complete instrumentation.

INTRODUCTION

It is recognized that the use of high-aspect-ratio blading in aircraft gas turbine compressors offers the potential of designing lighter, more compact units. The performance of such stages has not always been satisfactory, however, in that they have generally been found to have less weight flow range than similar stages with lower aspect-ratio blading (refs. 1 and 2). Reduced weight flow range typically results in reduced stall margin, especially in cases where the compressor must operate with inlet flow distortions.

The objective of this program is to investigate outer casing blowing and bleeding in order to determine their effectiveness in increasing the weight flow range of an isolated high-aspect-ratio rotor under conditions of distorted as well as undistorted inlet flow. The design of the rotor and of the blowing and bleeding devices is presented in reference 3.

The baseline performance of the rotor without casing boundary layer control is documented in reference 4. Indications that stalls initiate at the pitchline near the part-span shroud rather than at the tip for undistorted inlet flow conditions were obtained during the baseline performance testing. The stall point obtained at 100% speed in the baseline tests was at a flow of 172.2 lb/sec and a total pressure ratio of 1.48. Peak rotor adiabatic efficiency at design speed was 0.900.

This report presents the performance of the rotor when tested with a device for injecting high-energy air into the mainstream at the rotor tip. Stalling performance was obtained, both with and without blowing flow, for cases of undistorted inlet flow, inlet casing boundary layer trip, tip radial inlet distortion, and 90° one-per-rev circumferential distortion. Overall performance in each case was obtained with zero blowing flow and with that level of blowing flow which produced the highest stall line.

SYMBOLS

The following symbols are used in this report:

A flow area, in^2

A_j area represented by each discharge rake element. This is the area of an annulus bounded either by radii midway between those of the two adjacent elements or by the hub or casing, in^2

C_h enthalpy-equivalent static-pressure-rise coefficient,

$$C_h = \frac{2gJc_p t_1\left[\left(\frac{p_2}{p_1}\right)^{\frac{\gamma-1}{\gamma}} - 1\right] - (U_2^2 \quad U_1^2)}{V_1'^2}$$

C_p static - pressure-rise coefficient,

$$C_p = \frac{p_2 - p_1}{P_1' - p_1}$$

c_p specific heat at constant pressure, Btu/lb-°R

D diffusion factor

$$D = 1 - \frac{V_2'}{V_1'} + \frac{r_2 V_{\theta 2} - r_1 V_{\theta 1}}{2\bar{r}\,\sigma\, V_1'}$$

g acceleration due to gravity, 32.174 ft/sec^2

i incidence angle, difference between air angle and camber line angle at leading edge in cascade projection, deg

J mechanical equivalent of heat, 778.161 ft-lb/Btu

M Mach number

P total or stagnation pressure, psia

P_j arithmetic average total pressure at j immersion, psia

p static or stream pressure, psia

r	radius, in
$\bar{r}$	mean radius, average of streamline leading-edge and trailing-edge radii, in
T	total or stagnation temperature, °R
T_j	arithmetic average total temperature at j immersion, °R
t	static or stream temperature, °R
U	rotor speed, ft/sec
V	air velocity, ft/sec
V_{zj}	average axial velocity at j immersion, ft/sec
W	weight flow, lb/sec
z	displacement along compressor axis, in
β	air angle, angle whose tangent is the ratio of tangential to axial velocity, deg
γ	ratio of specific heats
δ	ratio: $\frac{\text{total pressure}}{\text{standard pressure}}, \frac{\text{psia}}{14.696 \text{ psia}}$
δ°	deviation angle, difference between air angle and camber line angle at trailing edge in cascade projection, deg
ε°	meridional angle, angle between tangent to streamline projected on meridional plane and axial direction, deg
θ	ratio: $\frac{\text{total temperature}}{\text{standard temperature}}, \frac{°R}{518.688°R}$
θ°	angular displacement about compressor axis, deg
η	efficiency
κ°	angle between cylindrical projection of the blade camber line at the leading or trailing edge and the axial direction, deg
ρ	static or stream density, lb-sec^2/ft^4
σ	solidity, ratio of chord to spacing
ψ	stream function; $\psi_h = 0$, $\psi_c = 1$
$\bar{\omega}$	total-pressure-loss coefficient

Subscripts:

ad	adiabatic
an	annulus value
avg	arithmetic average at any plane
c	casing at any plane
d	downstream
h	hub at any plane
in	inlet
j	immersion number
m	meridional direction
p	polytropic
s	suction surface
u	upstream
z	with respect to axial displacement
θ	with respect to tangential displacement
1	leading edge
2	trailing edge
0.05, 0.65, 0.90, 1.54, 1.90, 3.50	instrumentation plane designations (figures 4 and 5)

Superscripts:

*	critical flow condition
'	relative to rotor

APPARATUS AND PROCEDURE

Test Rotor Design

A high aspect-ratio transonic rotor was designed as an instrument for evaluating the effects on performance and operating range of casing blow and bleed devices on stages of this type. The overall characteristics of the rotor design are contained in the following list.

1. Rotor tip speed, 1120 ft/sec.
2. Inlet hub-tip radius ratio, 0.50.
3. Total-pressure ratio, 1.47, radially constant.
4. Corrected weight flow per unit annulus area, 39.32 lb/sec-sq ft.
5. Rotor tip solidity, 1.0.
6. Rotor tip relative Mach number, 1.2.
7. Rotor tip diffusion factor, 0.45.
8. Rotor blade aspect ratio, 4.5.
9. Rotor blade section; double-circular-arc on cylindrical sections.
10. Rotor chord, 1.772 in., radially constant.
11. Rotor maximum thickness-chord ratio, 0.085 at hub, 0.03 at tip.
12. Number of rotor blades, 60.
13. Rotor tip diameter, 34 inches.
14. Corrected weight flow, 187 lb/sec.

The rotor tip diffusion factor of 0.45 is somewhat higher than is common practice for stages with a radius ratio of 0.5. The moderately large tip loading was selected with the expectation that the boundary layer control devices to be investigated would permit operation at loading levels that exceed those given by conventional design criteria. The remaining items were selected as being typical of a compressor front stage, the stage most likely to require a boundary layer control device. Full details of the methods employed in the design of this rotor and the resulting design parameters are presented in reference 3.

Blowing Air System

The blowing air system supplied a measured quantity of preheated and regulated air to a plenum chamber at the tip of the rotor, and an insert in the compressor casing directed this air into the main airstream. A schematic of the air supply system is given in figure 1. The blowing air was preheated by passing a fraction of this air through a steam-air heat exchanger, and then mixing this fraction with the main supply. Varying the flow through the heater by means of proportional mixing valves allowed the desired blowing air temperature to be set. Flow through the system was measured by an orifice plate in the supply line, and was controllable by adjusting the plenum pressure by means of a control valve.

The blowing insert used in these tests contained three rows of tapered, converging - area holes. These holes were oriented so as to direct the blowing flow radially inward at a 20° angle from a cylindrical surface and also to impart 30° of counter-swirl (that is, the tangential component of the injected flow was opposite to the rotor's rotation). The first two rows of holes discharged foreward of the rotor's leading edge while the third row discharged over the rotor tip. The insert configuration is shown in figure 2. The area of the holes was set so that, with an assumed flow coefficient of 0.92, approximately 4% of design flow would be passed with the holes just choked. The temperature of the blowing flow was set as a function of the plenum pressure according to the relationship given in figure 3. This relationship was arrived at by assuming that the source of the blowing flow in an actual engine would be the rear stages of a multi-stage compressor. A ducting loss of 15% of the rear stage's total pressure and an overall adiabatic compression efficiency of 75% were assumed for the injected air in order to determine the blowing flow temperature. Additional discussion of the design of this blowing insert is found in reference 3.

Test Facility

Performance tests of this rotor were made in General Electric's House Compressor Test Facility at Lynn, Massachusetts. The general aspects of the test setup are shown in figure 4 of reference 4. The test rotor draws air from the atmosphere through two banks of filters. The first filter bank is intended to remove 22% of the particles larger than 3-5 microns (dust spot test). The second and final filter bank is intended to remove 90-95% of the remaining particles down to the same size. The air then passes through a coarse wire inlet screen and into the bellmouth. Outlet guide vanes downstream of the test rotor remove most of the swirl. In the exit assembly the air is split into two streams. The inner air stream is passed into an exit pipe which contains a flow straightener and a venturi flow meter, and is then exhausted to atmosphere. The outer air stream passes through a slide cylindrical throttle valve and into a collector. Two pipes, each of which contains a flow straightener and a venturi flow meter, then discharge the air to atmosphere.

Power to drive the test rotor is provided by a high-pressure non-condensing steam turbine rated at 15,000 horsepower.

Instrumentation

Schematic views of the instrumentation provided for the test are shown in figures 4 and 5, and photos of the rakes themselves are shown in figure 6. Inlet total temperature was measured by twenty-four (24) thermocouples distributed on the inlet screen. For the first test run described in this report, the inlet total and static pressures were measured at plane 0.05 by six pitot-static rakes having seven elements each, figure 6(a). These seven elements were placed radially at centers of equal annulus area. During all later test runs, four 5-element inlet distortion total-pressure rakes, figure 6(e) located at plane 0.65 were used to obtain the inlet total pressure. A 15-element boundary layer rake, figure 6(b), was immersed from the outer casing at plane 0.65 ahead of the rotor.

Hot wire anemometer data were taken with three shielded probes, figure 6(f), located behind the rotor at plane 1.54. These were used to obtain traces on high-speed paper tape from which the number, rotative speed, and radial extent of the rotating stall cells could be determined.

Outlet total pressures and temperatures were measured at plane 1.9 by 4 fixed rakes of each type, figures 6(c) and 6(d). Immersions of the five elements on each rake corresponded to the design streamlines at the 10%, 30%, 50%, 70%, and 90% annulus height positions, as measured from the tip at plane 1.54. The discharge rakes at plane 1.9 were ahead of the outlet guide vanes, and thus had to measure swirling flow. These rakes were therefore rotated 37.5° from the axial direction to match the pitchline swirl angle of the flow at the design condition.

A generous number of static pressure taps was located on the hub and casing throughout the flowpath. At measuring planes where the fixed rakes were located, static pressures at the hub and casing were measured at more than one circumferential position, (figure 5).

Distortion Screens and Boundary Layer Trip

Two inlet airflow distortion patterns were tested with this blowing insert configuration. These were produced by mounting distortion screens at plane 0.10 located approximately 26% of a rotor diameter ahead of the rotor's leading edge. The circumferential screen covered a 90° arc of the inlet annulus from hub to tip, while the radial distortion screen covered the outer 40% of the inlet annulus area. Figures 7(b) and 7(c) show the general layout of the screens. Both were designed to produce patterns at plane 0.65, the inlet instrumentation station, which had a value of $(P_{max} - P_{min})/P_{max} = 0.20$ at the design flow of 187 lb/sec; accordingly both were made of 20 mesh, 0.016-inch wire diameter screen material which had approximately 54%

blocked area. The distortion screens were mounted on a support screen which covered the entire annulus and which was made of 0.092 inch diameter wire at 3/4-inch spacing.

The boundary layer trip was installed briefly during the first test run; it is shown in figure 7(a). It was used to thicken the inlet casing boundary layer, and consisted of a sharp-edged annular ring protruding 0.30 inch into the airstream from the casing at plane 0.10. During previous testing (reference 4), the use of the boundary layer trip increased the inlet casing boundary layer displacement thickness from 0.035 inch to 0.29 inch at design speed and flow.

Test Procedure

The first test run on this blowing insert configuration was a preliminary investigation of the operation of the blowing system and the effect of blowing on stall performance. Tests were conducted during this first run with undistorted inlet flow with and without the inlet boundary layer trip installed. For these tests, the inlet total pressure was obtained from six pitot-static rakes located at plane 0.05. Data obtained consisted of numerous stalls at various blowing rates and enough overall performance data points to define general performance trends. Based on this limited amount of data, it was concluded that stalls originated at the pitchline with and without the boundary layer trip as had been observed in tests with the plain casing insert, reference 4. Furthermore, the use of blowing at the tip produced only a small gain in stall performance, with the greatest gain at the largest blowing flow rates.

Because of these results, it was decided to test this blowing insert configuration with inlet distortions and no boundary layer trip. It was anticipated that stalls would then initiate at the tip, and the use of blowing might produce larger gains in stall performance. Tip radial and 90° circumferential inlet distortion patterns were tested in this second phase. The final phase of the testing was a complete test with undistorted inlet flow. During all the inlet distortion and final undistorted inlet testing, the inlet total pressure was obtained from the four 5-element inlet distortion rakes located at plane 0.65 aft of the plane of the distortion screen.

The first part of each test was devoted to determining the stall line at three different blowing flow rates and a base stall line with zero blowing flow. Corrected speeds of 70%, 90%, and 100% were investigated. Following this, the compressor performance at each of these three speeds was mapped for zero blowing flow and also for that blowing flow rate which produced the best stall performance. To complete each test, rotating-stall and stall-removal overall performance readings were obtained at each speed with both zero and optimum blowing flow rates.

Stall Testing The first part of each test sequence was preliminary stall testing to determine the stall line with zero blowing flow and with three different blowing flow rates. These stall points were established by setting the blowing plenum pressure and temperature at a point well removed from stall and then slowly closing the throttle valve until strain gage and hot wire anemometer signals indicated the formation of rotating stall cells. In two instances at 70% speed with radial distortion and high blowing flows, throttling was terminated by strain gage indications of incipient blade aeromechanical instability. After each of these preliminary stalls, the throttle valve was set at a position as close as possible to stall, and an overall performance data reading was taken in order to better define the exact conditions at the stall line. For each of these preliminary stalls three shielded hot wire anemometers were immersed to the 10%, 50% and 90% positions and traces of the rotating stall cells were obtained on high-speed paper tape. Examination of these traces indicated the radial extent of the stall cells.

At the end of each test, the vehicle was stalled again at each speed with zero and optimum blowing flow rates. During this final stall, all three hot wires were set at the immersion where the stall cells were strongest in the first stall. From the resulting tapes, information on the number and speed of the rotating stall cells could be obtained by the methods explained in reference 4. While throttling into and out of this second stall, an ICPAC* trace was obtained. Conditions were stabilized in stall and a rotating-stall overall performance reading was taken. When this was completed, the speed was maintained and the discharge throttle valve slowly opened until the stall cleared; at this condition a stall-removal overall performance reading was taken.

The discharge throttle valve was geared for a fast opening-closing rate for the first stall testing and was closed in a stepwise fashion by the operator. During the second stalls the discharge valve was geared to move very slowly and was actuated by the operator at a constant rate so that the stall line would always be obtained in a fully consistent manner.

Testing in the Unstalled Region The throttle settings at which data were taken in the stall-free region of operation were selected to give an approximately even spacing of the points on the compressor performance map speed lines. All vehicle temperatures and pressures were recorded in digital form on punched paper tape for computerized data reduction.

When taking overall performance data with the optimum blowing flow rate, it was necessary to duplicate the optimum blowing flow conditions which had been set during preliminary stall testing. This was done by setting the speed, throttle position, blowing pressure and blowing temperature to the same values which had existed during the overall performance data point

*Instantaneous Compressor Performance Analysis Computer. This is an analogue circuit which senses weight flow and pressure ratio, and which plots these quantities nearly instantaneously to provide an approximate on-line compressor performance map.

recorded in conjunction with the preliminary stall at optimum blowing flow. Several more overall performance points were then taken between this match condition and maximum flow without making further adjustments to the blowing air flow system. This procedure was followed for 70%, 90%, and 100% speeds.

For overall performance data points the inlet total pressure was determined by taking the arithmetic average of all elements on the inlet total-pressure rakes. The discharge total-pressure and total-temperature ratios were obtained by the mass-weighting procedure explained in reference 4. Although the above methods of obtaining inlet and discharge conditions cannot really be justified for the case of a circumferential inlet distortion, these methods were judged to be as good as any other that could be easily applied with the available data. Therefore these techniques were retained for all inlet conditions.

When overall performance was computed for data points where blowing air was being injected, no attempt was made to correct the calculated discharge quantities or the efficiency for the enthalpy added to the main discharge stream by the blowing air. In some instances high-temperature blowing air was sensed by the discharge thermocouple rakes and the discharge mass-weighting procedure computed a very high tip tangential component of velocity and thus a very low tip axial component. This resulted in unrealistic weighting being given to the various radial measuring positions. In general, it is believed that this effect is slight in respect to the discharge total-pressure ratio calculations, but has affected the discharge total temperature and efficiency calculations. As a result, the adiabatic efficiency for data points with blowing flow has not been tabulated or plotted on the performance maps.

The weight flow was taken to be the inlet flow ahead of the plane of blowing air injection. This was obtained by subtracting the blowing air flow (as measured by an orifice in the supply system) from the total weight flow measured by the test vehicle discharge venturi meters. Both inlet weight flow and blowing weight flow were corrected by the same $\sqrt{\theta}/\delta$ term, as obtained from average inlet conditions.

RESULTS AND DISCUSSION

The results reported herein were obtained with blowing insert configuration no. 1 in order to evaluate the effects of outer case blowing over the tip of a transonic rotor. The basic performance of the rotor with a solid casing and no tip boundary layer control is documented in reference 4. The present blowing configuration was tested with undistorted inlet flow, with an inlet casing boundary layer trip, and with circumferential and radial inlet flow distortions. The overall and stall performance of each inlet flow condition is presented and discussed separately in the following sections for the cases of zero and optimum blowing flow rate.

Undistorted Inlet Testing

Determination of Stall Limits The performance map for undistorted inlet flow is shown in figure 8. Three stall lines are shown on the performance map: blowing insert configuration with zero blowing flow, blowing insert configuration with optimum blowing flow, and plain casing insert configuration (reference 4). The stall lines on the map were based on those stalls for which the most reliable ICPAC readings were available, Table 1(a). The stalling weight flow was determined by recording the approximate flow as given by the ICPAC system at the instant stall was detected, and then by correlating ICPAC flow values with the actual weight flows measured during overall performance data points. Stalling total-pressure ratio was obtained by extrapolating the speed line on the performance map using the ICPAC trace as a guide.

Table 1(a) is a listing of conditions at the limit of stall-free operation for each stall point obtained in undistorted inlet testing. The stalls numbered 1-8 were performed during the first test run in the series and indicated that, although the improvement due to blowing was not large, the higher blowing rates tended to produce the most improvement in stall-free weight flow range. From these results, it was decided that the optimum blowing rate was the maximum blowing flow which the system could supply, about 10 lb/sec. The performance map (figure 8) thus displays the stall line and overall performance obtained with the above blowing flow; stalls numbered 12-17 in Table 1(a) were obtained with this optimum blowing flow during the later more complete undistorted inlet testing. The particular stall points used to define the zero blow and optimum blow rate stall lines on the performance map are indicated in Table 1(a).

Hot-wire anemometer traces obtained at the 10%, 50% and 90% immersions during the first stalls at various blowing rates indicated that both with and without blowing flow the stalls at each speed were most severe at the 50% immersion. This duplicated the trend found in plain casing insert undistorted inlet testing (reference 4), and gave further support to the belief that the stalls initiated near the part-span shroud.

The effect of the blowing insert itself upon the stall line may be seen by comparing the zero blowing flow and the plain casing insert stall lines in figure 8. Approximately 4-6 lb/sec additional flow range was gained by replacing the solid casing insert with the blowing insert, even when no blowing air was injected. This improvement in stall-free range due to the change in casing configuration is greater than the improvement of 2-3 lb/sec due to the injection of blowing air at the tip. Since the stalling flow was generally repeatable to within 2-3 lb/sec, it must be concluded that the presence of holes in the casing insert did indeed alter the flow pattern enough to delay the onset of rotating stall. This result was unexpected in view of the fact that hot wire anemometer traces taken during the stalls in this test and in previous plain casing insert tests indicated that the stalls were initiating in the region of the part span shroud, not at the rotor tip.

One possible mechanism by which the presence of holes in the casing might have delayed stall when no air was injected is that of recirculation in and out of the holes. Figure 9 shows that the pressure in the plenum chamber is intermediate between the casing static pressures immediately upstream of the rotor leading edge and downstream of the trailing edge. Thus the pressure differences across the foreward and aft rows of holes are in the proper direction to support a recirculation pattern in which flow enters the plenum chamber through the rear row of holes and re-enters the main flow path by way of the holes farther foreward. It would appear unlikely, however, that any recirculated air re-entering through the foreward holes could act as a self-induced blowing flow which increased stall margin by increasing the inlet dynamic head of the flow relative to the rotor tip. This is the presumed mechanism when blowing air is injected, but any recirculated air would enter the main stream at a much lower velocity than would blowing air and thus should be less effective not more effective.

A more plausible mechanism is that by allowing recirculation in the circumferential direction or by some resonator effect, the holes are able to suppress the substantial circumferential variations in static pressure which are necessary in order for rotating stall cells to exist in a rotor. If these circumferential variations in static pressure exist at all radii ahead of the rotor, suppressing them at the tip would also reduce them at other radial positions. This could result in delaying the formation of rotating stall cells at the pitchline.

Performance in Stall The overall performance data points recorded while the rotor was operating with rotating stall present appear as solid symbols in figure 8 and are denoted by (RS) in Tables 1 and 3. Since conditions are quite unsteady when operating in stall, the accuracy of these readings is open to question. After each rotating-stall overall performance reading was taken, speed was maintained and the discharge throttle valve was slowly opened until the stall cleared. At this setting a stall-removal overall performance reading was taken; these points appear as half-shaded symbols in figure 8, and are denoted by (SR) in Table 3. In general, there is some hysteresis in this process: the stall does not clear until the flow increases above that at which stall first appeared. There was more of this hysteresis at the higher speeds than at the lower, and blowing at the tip tended to reduce the hysteresis.

While recording overall performance data with stalls present, three shielded hot-wire anemometers were immersed to the 50% position and traces of the stall cell patterns were obtained. From these the number and rotative speed of the rotating stall cells could be determined; these data are tabulated in Table 2(a).

Unstalled Overall Performance Tabulations of all overall performance data points taken during undistorted inlet flow testing are given in Table 3. Table 3(a) lists data points taken during the first test run, while Table 3(e) lists those points taken during subsequent complete performance tests. The compressor performance map, figure 8, is based on the data from the complete performance testing, and indicates performance for both zero blowing and optimum blowing flow. Optimum blowing flow rate was determined during the first test run to be the maximum flow the system could supply, about 10 lb/sec. Symbols on the performance map having an "X" through them indicate data taken with optimum blowing flow.

The flow scale on the performance map is vehicle inlet flow, and does not include the amount of blowing air injected. Plotted in this manner, the map shows that the addition of blowing air reduces the maximum inlet weight flow capacity of the rotor by about 4-5 lb/sec, although discharge weight flow has increased due to the 10 lb/sec of added blowing air. With zero blowing flow, the pressure versus flow relationship at each speed is essentially the same as that recorded in previous plain casing insert configuration tests (reference 4).

The adiabatic efficiencies plotted in figure 8 are for zero blowing flow only. As discussed in the Test Procedure section, the data analysis method used to compute adiabatic efficiency was not capable of giving a meaningful answer when the high-pressure, high-temperature blowing air was injected. On the map, a comparison is given between the zero blowing flow efficiencies and those from plain casing insert configuration tests. A marked reduction in adiabatic efficiency occurred at all speeds. This reduction in efficiency was not noted during the first test run; indeed, Readings 1-3 tabulated in Table 3 (a) show that the efficiency at all speeds was approximately one point higher during the first test than observed in plain casing insert testing. The most probable cause of the reduced efficiency is dirt on the blades. The vehicle had been operated for five days of distortion testing between the first test run and the final undistorted inlet test, and the blowing system had been in use for all these intervening runs. In addition, water at one time entered the blowing system through a crack in the steam-air heat exchanger. At the end of testing, deposits of rust and dirt were found on the blades. The high efficiencies recorded during the first test run also are somewhat suspect in that one discharge total temperature rake was reading low on several of its elements throughout the first run. This problem was corrected before proceeding with later performance tests. In general, the efficiency data are not reliable enough to assess the efficiency penalty, if any, caused by the blowing insert configuration.

Boundary Layer Trip Testing

The inlet casing boundary layer trip, shown in figure 7(a), was installed only during the first test run. The vehicle was stalled several times with and without blowing flow at each of 90% and 100% speeds, and overall performance was recorded near these stall points. Table 1(b) is a listing of conditions at the points where the stalls occurred. The Table 3(b) tabulates the overall performance points that were recorded. The compressor performance map for the boundary layer trip tests is given in figure 10.

Three stall lines are shown in figure 10: the solid line is for zero blowing flow and the dotted line is with blowing, both of these with the boundary layer trip installed; the dashed line represents the undistorted inlet stall line for zero blowing flow from figure 8. The particular stall points used to determine the stall lines are indicated in Table 1(b). Comparison of the zero blowing stall lines in figure 10 for boundary layer trip and undistorted inlet tests shows that the presence of the boundary layer trip causes a slight reduction in the stall line. Blowing at the casing with the boundary layer trip installed causes the stalling weight flow to decrease by 3-5 lb/sec, a somewhat larger improvement than obtained with undistorted inlet. The effect of varying the blowing flow rate was not well established in that all stalls with blowing were made with nearly maximum flow, and the minor changes that were made in the blowing rate produced inconclusive results.

Hot-wire anemometer traces were obtained at each stall point to indicate the radial extent of the stall cells. As with undistorted inlet, and also in previous plain casing insert configuration tests (reference 4), the stall hot wire traces indicated that stalls initiated at the pitchline near the part-span shroud. No rotating-stall or stall-removal overall performance data points were recorded.

The adiabatic efficiency of the rotor with the boundary layer trip and zero blowing flow is shown in figure 10 compared to that obtained with zero blowing flow without the boundary layer trip. However, the data for the case of no boundary layer trip was obtained with dirty blades, and appears to be unrealistically low. A comparison of two 100% speed, zero blow overall performance data points taken during the first tests when the blades were clean (Reading 3 in Table 3(a) and Reading 9 in Table 3(b)) indicates that the rotor efficiency with boundary layer trip has dropped about 3.5 points relative to that for no boundary layer trip.

Because blowing at the casing had rather little effect on stall performance with the boundary layer trip installed, it was decided not to conduct a complete performance test with this inlet condition.

Radial Distortion Testing

The screen used to produce the tip radial inlet distortion pattern is shown in figure 7(b). This screen covered the outer 40% of the inlet annulus

area at plane 0.10. Two of the five elements on each inlet distortion total pressure rake were thus located in the region of distorted inlet flow.

A complete performance test was conducted with the tip radial inlet distortion condition.

Determination of Stall Limits Table 1(d) is a listing of conditions at the limit of stall-free operation for each stall point obtained in radial inlet distortion testing. These data indicated that the optimum blowing flow, that giving the greatest improvement in unstalled operating range, was the largest blowing rate obtained, about 10 lb/sec. The compressor performance map for radial distortion testing is presented in figure 11. The zero blowing and optimum blowing rate stall lines are shown, as well as undistorted inlet zero blowing stall line from figure 8. It should be noted that the limit of operation at 70% speed with maximum (or optimum) blowing flow was due to stress limits which indicated incipient blade aeromechanical instability rather than rotating stall. The particular stall points used to generate the radial distortion stall lines are indicated in Table 1 (c).

Hot-wire anemometer traces at 10%, 50% and 90% immersions obtained during the initial stalls are shown in figure 12. These indicated that the rotating stall cells extended over the outer span of the blades and were most severe at the tip; this was true for all points where rotating stall occurred,both with and without blowing. In attempting to clear the stalls with zero and minimum blowing flow by opening the discharge throttle valve, the rotating stall cells cleared at the pitch and hub but not at the tip; it was necessary to drop speed in order to clear the rotating stall from the tip. The stalls could be cleared without dropping speed at the two higher blowing flow rates. From these observations, it is relatively certain that rotating stalls initiated at the tip with radial inlet distortion. Because of these tip stalls, the injection of air at the tip was able to energize the weakest part of the flow and produce the comparatively large improvement in stall performance seen in figure 11.

Performance in Stall Rotating-stall overall performance data points were obtained whenever blade stress limits allowed, and stall-removal points were obtained when the stalls could be cleared without reducing speed. These data points appear in figure 11 as solid and half-shaded symbols. Although their accuracy is questionable due to the unsteadyness of the flow with rotating stall present, they do indicate the magnitude of performance loss caused by the rotating stall cells and the hysteresis involved in clearing the stalls.

While recording data in the stalled mode of operation, the three shielded hot-wire anemometers were immersed to the 10% position where the rotating stall cells had been most severe in earlier stall testing. Traces of the stall cell patterns were obtained, and from these the number and rotative speed of the stall cells were determined. These data are tabulated in Table 2 (b).

Unstalled Overall Performance A tabulation of all overall performance data points taken during radial distortion testing is given in Table 3(c). The compressor performance map, figure 11, is based on overall performance data points with zero and maximum, or optimum, blowing rates. Some of the zero and maximum blowing flow data points in Table 3(c) were not plotted in figure 11 in order to avoid crowding too many data points into the limited weight flow range investigated at each speed; the ommitted data points are so indicated in the table. As in undistorted inlet testing, the rotor adiabatic efficiency for data points with blowing was not plotted.

Figure 13 presents plots of inlet and discharge total pressures and discharge total temperatures for Reading 16, a data point near stall at 100% speed and with zero blowing flow. At this condition, the radial inlet distortion screen created a pattern at the inlet measuring station, plane 0.65, which had a value of the distortion parameter $\frac{P_{max} - P_{min}}{P_{max}}$ equal to about 0.17. The average total pressures in the distorted and undistorted regions were used to determine the above value.

The harmful effects of the radial distortion on stall performance are immediately apparent in figure 11; however, the fact that total pressure ratio was higher than the undistorted inlet tests results at 70% and 90% speed was unexpected. An examination of the unreduced data and approximate calculation of mass-averaged inlet total pressure were made but failed to turn up any discrepancies in the overall performance as reported.

Circumferential Distortion Testing

The screen used to produce the circumferential inlet distortion pattern is shown in figure 7(c). This screen covered a 90° arc of the inlet annulus at plane 0.10, and was placed so that its centerline was at bottom center in the test vehicle. One of the four inlet distortion total pressure rakes, that at 196° from top center, was thus located in the region of distorted inlet flow.

A complete performance test was conducted with the circumferential inlet distortion condition.

Determination of Stall Limits Table 1(d) is a listing of conditions at the limit of stall-free operation for each stall point obtained in the circumferential distortion testing. These data indicated that the optimum blowing flow rate at each speed was the maximum available, about 10 lb/sec. The circumferential inlet distortion compressor performance map, figure 14, shows the stall lines for zero and optimum blowing flow rates, plus the undistorted inlet zero blow rate stall line from figure 8. The circumferential distortion stall lines in figure 14 were based on the rotating stall testing during which the slow discharge throttle valve drive was used. These particular stall points are numbered 13-18 in Table 1(d).

The stalling performance of the rotor subjected to this circumferential inlet distortion pattern was unusual, and was contrary to experience with other isolated transonic rotors, reference 5, as well as aircraft engine experience. Even without blowing at the tip, the unstalled range of operation was substantially increased with respect to the undistorted inlet condition. Although the stalling total-pressure ratio was reduced, the reduction in stalling weight flow was so large that the stall line plotted considerably to the left of the undistorted inlet stall line. The injection of blowing air at the tip produced a further substantial increase in unstalled weight flow range. However, the limited sample of inlet and discharge conditions obtained makes it impossible to determine the causes of this unusual stalling performance with circumferential distortion.

Hot-wire anemometer traces obtained at the 10%, 50% and 90% immersions during the initial stalls are shown in figure 15. These indicated that the rotating stall cells extended over the full span of the blades and were most severe at the tip both with and without blowing. The initiation of stall was not abrupt as in previous testing, but instead began with rotating stall cells forming intermittently until the throttle valve was closed beyond the point where stall was first observed. The rotating stall cells cleared very rapidly when the throttle was opened. Evidence from the hot-wire anemometer traces thus indicates that rotating stalls first formed at the tip in a highly unstable manner. Blowing at the tip was quite effective in delaying the breakdown of the flow at the casing and the formation of rotating stall cells.

Performance in Stall Rotating-stall and stall-removal overall performance data points were recorded with and without blowing at 70%, 90%, and 100% speeds. Although their accuracy is questionable due to the unsteadyness of the flow with rotating stall cells present, these data do indicate that the decrease in performance caused by the formation of stall cells is greater and that there is more hysteresis involved in clearing the stalls without blowing than when blowing air is injected.

The number and rotative speed of the stall cells were determined from hot-wire anemometer traces obtained at the 10% immersion while the vehicle was operated in stall; these data are tabulated in Table 2 (c). In some instances the number of stall cells was observed to change while the vehicle was stabilized in the stalled mode of operation, giving further evidence of the unstable stall mode with this inlet distortion condition.

Unstalled Overall Performance A tabulation of all overall performance data points taken during circumferential inlet distortion testing is given in Table 3(d).The compressor performance map, figure 14, is based on overall performance data points with zero and maximum, or optimum, blowing flow rates. As in the other phases of this test, the rotor adiabatic efficiency for data points with blowing was not plotted.

Figure 16 presents plots of inlet and discharge conditions for Reading 86, a data point at 100% speed with zero blowing flow. At this operating point, the circumferential inlet distortion screen created a pattern at the inlet

measuring station, plane 0.65, which had a value of the distortion parameter $\frac{P_{max} - P_{min}}{P_{max}}$ equal to about 0.13. The average total pressures in the distorted and undistorted regions were used to determine the above value.

The large reductions in rotor adiabatic efficiency and the large decreases in flow and pressure rise capability at each speed seen in figure 14 point to the existence of large losses being generated in the flow. This, plus the unusual stall performance with circumferential distortion suggested that further testing with much more extensive instrumentation was needed. Such testing was performed on a later configuration, and the results obtained will be presented in a subsequent report.

REFERENCES

1. Kussoy, Marvin I., and Bachkin, Daniel: Comparison of Performance of Two Aerodynamically Similar 14-Inch Diameter Single Stage Compressor Rotors of Different Chord Length, NACA RM E57I03, 1958.

2. Swan, W.C.: An Experiment with Aspect Ratio as a Means of Extending the Useful Range of a Transonic Inlet Stage of an Axial Flow Compressor, Journal of Engineering for Power, Trans. ASME, Series A, Vol. 88, 1966, pp. 1-12.

3. Giffin, R.G., and Smith, L.H., Jr.: Experimental Evaluation of Outer Case Blowing or Bleeding of Single Stage Axial Flow Compressor, Part I - Design of Rotor and Bleeding and Blowing Configurations, NASA CR-54587, 1966.

4. Koch, C.C., and Smith, L.H., Jr.: Experimental Evaluation of Outer Case Blowing or Bleeding of Single Stage Axial Flow Compressor, Part II - Performance of Plain Casing Insert Configuration with Undistorted Inlet Flow and Boundary Layer Trip, NASA CR-54588, 1968.

5. Seyler, D.R., and Gostelow, J.P.: Single Stage Experimental Evaluation of High Mach Number Compressor Rotor Blading, Part II - Performance of Rotor 1B, NASA CR-54582, 1967.

Table 1 (a). - Summary of Stall Points from ICPAC System for Undistorted Inlet Testing

Stall Number	Corrected Speed, % Design	Throttle Valve Setting	ICPAC Flow	Inlet Corrected Flow lbs/sec	Blowing Corrected Flow lbs/sec	Blowing Air Plenum P, psia	Blowing Air Plenum T, °R	Plane 0.9 Casing Static p, psia	Associated Reading No. of Table 3.
1	70	5.05	106.3	119.7	0	14.1	548.6	13.7	1
2	90	6.0	144.2	159.2	0	13.4	569.0	12.9	2
3	100	5.3	155.7	171.2	0	13.4	596.6	12.6	3
4	70	6.0	103.3	116.5	4.0	-	-	-	-
5	70	6.7	102.2	115.3	6.2	18.5	595.7	13.8	4
6	90	6.8	144.4	159.5	5.4	-	-	-	-
7	100	6.0	154.5	170.0	5.3	-	-	-	-
8	100	6.8	154.4	169.9	7.4	21.0	621.0	12.8	5
9	70	4.9	116.2	115.1	0	-	-	-	-
10	90	6.05	154.8	154.8	0	13.6	584.2	13.0	108
11*	100	5.4	167.8	167.8	0	13.7	607.0	12.7	109
12*	100	7.4	166.4	166.5	8.9	23.4	650.2	12.9	110
13*	90	8.35	153.6	153.6	9.0	23.3	651.5	13.2	111
14	70	7.3	115.3	116.5	8.8	23.0	647.7	13.8	112
15*	70	7.3	115.0	116.2	8.8	23.2	649.4	13.8	113 (RS)
16	90	8.2	156.0	156.2	8.9	23.3	651.0	13.2	115 (RS)
17	100	7.25	165.7	165.7	8.9	23.5	654.0	12.9	117 (RS)
18	100	5.3	168.5	168.5	0	14.0	640.3	12.7	119 (RS)
19*	90	6.0	155.2	155.2	0	13.9	609.7	13.0	121 (RS)
20*	70	5.0	117.4	118.4	0	14.3	583.9	13.8	123 (RS)

*Points used to establish stall lines on performance map.

(RS) indicates a rotating-stall overall performance reading.

Table 1 (b). - Summary of Stall Points from ICPAC System for Boundary Layer Trip Testing

Stall Number	Corrected Speed, % Design	Throttle Valve Setting	ICPAC Flow	Inlet Corrected Flow lbs/sec	Blowing Corrected Flow lbs/sec	Blowing Air Plenum P, psia	Blowing Air Plenum T, °R	Plane 0.9 Casing Static p, psia	Associated Reading No. of Table 3
1*	100	6.0	141.8	165.8	8.2	21.1	623.9	12.7	6
2	90	7.3	132.5	155.0	8.1	21.1	621.3	13.0	7
3*	90	5.4	132.4	157.0	0	13.9	587.4	13.0	8
4*	100	4.7	143.0	168.6	0	13.8	605.4	12.8	9
5	100	5.3	141.8	165.2	7.6	-	-	-	-
6*	90	6.0	130.6	151.0	7.5	16.9	562.9	13.1	10

Table 1 (c). - Summary of Stall Points for Radial Distortion Testing.

1	70	17.8	117.4	126.9	0	14.1	580.9	13.4	13
2	90	21.6	148.5	170.2	0	13.3	615.1	12.0	14
3	100	26.0	153.4	177.4	0	13.1	639.2	11.7	16
4*	70	18.8	118.3	128.2	0	14.1	575.7	13.4	28 (RS)
5*	90	22.6	148.8	170.5	0	13.6	605.5	12.0	30 (RS)
6*	100	24.0	152.9	176.5	0	13.3	632.4	11.7	31 (RS)
7	100	18.4	150.8	172.6	3.9	16.5	551.0	12.1	33
8	90	16.6	145.7	165.9	3.9	16.2	552.2	12.3	34
9	70	16.5	114.0	121.5	3.6	15.6	550.9	13.5	35
10*,**	70	10.6	106.3	111.8	10.3	24.3	659.2	13.7	36
11	90	17.3	146.6	164.4	11.0	25.8	671.9	12.4	37
12	100	14.0	148.5	167.8	11.0	25.9	673.2	12.3	38
13	100	15.0	149.4	169.4	7.4	19.7	610.3	12.2	39
14	90	16.1	145.4	164.4	7.0	19.5	613.9	12.4	40
15**	70	12.0	110.0	117.0	5.9	18.2	604.8	13.6	41
16*	90	17.3	146.7	165.0	9.2	25.3	680.5	1 2.4	54 (RS)
17*	100	14.3	149.2	169.2	9.3	25.1	682.8	12.2	56 (RS)

*Points used to establish stall lines on performance map.
**Stability limit.

(RS) indicates a rotating-stall overall performance reading.

Table 1 (d). - Summary of Stall Points from ICPAC System for Circumferential Distortion Testing

Stall Number	Corrected Speed, % Design	Throttle Valve Setting	ICPAC Flow	Inlet Corrected Flow lbs/sec	Blowing Corrected Flow lbs/sec	Blowing Air Plenum P, psia	Blowing Air Plenum T, °R	Plane 0.9 Casing Static p, psia	Associated Reading No. of Table 3.
1	70	4.45	95.6	100.5	0	14.6	571.5	13.9	59
2	90	5.75	121.4	130.0	0	14.3	589.2	13.3	62
3	100	5.8	132.2	143.7	0	14.2	617.8	13.0	64
4	70	3.2	89.0	93.5	2.9	15.8	558.3	14.0	65
5	90	6.2	120.8	128.5	3.4	16.1	556.4	13.4	66
6	100	6.0	131.0	142.5	3.2	16.2	554.2	13.0	67
7	100	6.6	127.8	137.0	9.9	24.4	681.7	13.2	68
8	90	4.6	109.7	115.0	9.7	23.5	664.7	13.7	69
9	70	2.7	80.5	85.2	7.8	23.0	664.4	14.1	70
10	70	2.1	83.6	88.5	5.8	18.2	605.1	14.1	71
11	90	6.25	118.4	126.5	6.2	18.8	609.4	13.4	72
12	100	5.95	128.2	138.0	6.5	19.3	622.9	13.2	73
13*	100	5.7	125.6	135.2	8.6	23.7	691.4	13.2	74 (RS)
14*	90	5.04	111.3	118.1	8.4	23.4	678.9	13.6	76 (RS)
15*	70	2.8	82.1	86.8	8.5	23.1	675.9	14.1	78 (RS)
16*	70	4.55	96.8	101.8	0	14.9	615.9	13.9	80 (RS)
17*	90	5.7	122.2	130.7	0	14.9	627.9	13.3	82 (RS)
18*	100	5.5	130.8	142.2	0	14.9	648.7	13.0	84 (RS)

*Points used to establish stall lines on performance map.
(RS) indicates a rotating-stall overall performance reading.

Table 2. - Tabulation of Rotating Stall Cell Data.

Corrected Speed, % Design	Throttle Valve Setting	Rotating Stall Rdg. No.	Number of Stall Cells	Stall Cell Speed / Rotor Speed	Radial Extent of Stall Cell
(a). Undistorted Inlet Testing.					
70	5.0	123	1	.280	inner 50% +
70*	7.3	113	1	.274	inner 50% +
90	6.0	121	1	.363	full span
90*	8.2	115	1	.370	full span
100	5.3	119	1	.550	full span
100*	7.3	117	1	.380	full span
(b). Radial Distortion Testing.					
70	18.7	28	3	.585	outer 50%
90	22.5	30	3	.588	outer 50%
90*	17.3	54	2	.716	tip
100	24.0	31	2	.588	outer 50%
100*	14.3	56	3	.506	tip
(c). Circumferential Distortion Testing.					
70	4.6	80	2 & 3	.579 & .580	outer 50%
70*	2.8	78	1	.594	outer 50%
90	5.7	82	1 & 2	.594 & .580	full span
90*	5.0	76	1	.711	full span
100	5.5	84	3	.569	full span
100*	5.7	74	4	.613	full span

Rotating stall data with optimum blowing flow. Entries not marked are for zero blowing flow.

Table 3 (a). - Overall Performance for Preliminary Undistorted Inlet Testing.

Rdg.	Total Pressure Ratio	Rotor Adiabatic Efficiency	Inlet Corrected Flow, lbs/sec	Corrected Speed, % Design	Throttle Valve Setting	Blowing Corrected Flow lbs/sec	Blowing Air Plenum P, psia	Blowing Air Plenum T, °R	Plane 0.9 Casing Static p, psia
1	1.201	.911	125.8	70.12	6.2	0	14.1	548.6	13.6
2	1.357	.949	166.2	90.15	7.0	0	13.4	569.0	12.7
3	1.463	.910	177.8	100.12	6.3	0	13.4	596.6	12.4
4	1.204	-	120.7	70.09	7.5	6.2	18.5	595.7	13.8
5	1.472	-	174.9	100.07	7.5	7.4	21.0	621.0	12.7

Table 3 (b). - Overall Performance for Preliminary Boundary Layer Trip Testing.

6	1.468	-	171.9	100.07	7.0	8.3	21.1	623.9	12.6
7	1.364	-	159.6	90.03	8.1	8.2	21.1	621.3	12.9
8	1.364	.905	162.2	90.12	6.3	0	13.9	587.4	12.7
9	1.464	.877	175.3	100.09	5.7	0	13.8	605.4	12.8
10	1.362	-	157.9	90.04	7.0	7.7	16.9	562.9	12.9

Table 3 (c). - Overall Performance for Radial Inlet Distortion Testing.

12	1.198	.912	141.4	70.09	51.0	0	13.6	564.2	13.0
13	1.204	.894	128.8	70.10	19.0	0	14.1	580.9	13.4
14	1.364	.907	172.1	90.15	25.0	0	13.3	615.1	12.0
16	1.406	.829	177.9	100.23	28.0	0	13.1	639.2	11.7
17*	1.401	.829	178.7	100.14	30.5	0	13.0	638.2	11.6
18	1.376	.812	181.2	100.16	50.0	0	12.7	627.4	11.5
19*	1.200	.914	137.4	70.09	30.0	0	13.8	565.9	13.1
20	1.202	.903	134.0	70.10	24.0	0	13.9	571.7	13.2

*Data points not appearing in figure 11.

Table 3 (c). (Continued)

Rdg.	Total Pressure Ratio	Rotor Adiabatic Efficiency	Inlet Corrected Flow, lbs/sec	Corrected Speed % Design	Throttle Valve Setting	Blowing Corrected Flow lbs/sec	Blowing Air Plenum P, psia	Blowing Air Plenum T, °R	Plane 0.9 Casing Static p, psia
21*	1.203	.904	130.5	70.07	21.0	0	14.1	575.8	13.3
22	1.336	.889	174.9	90.16	50.0	0	12.8	597.3	11.7
23*	1.349	.897	174.0	90.14	33.0	0	13.0	604.0	11.8
24	1.354	.904	173.4	90.15	30.0	0	13.1	608.6	11.9
25*	1.359	.908	172.6	90.14	27.0	0	13.2	612.8	11.9
26	1.395	.827	180.0	100.11	33.0	0	12.9	630.4	11.6
27*	1.403	.832	178.6	100.09	29.0	0	13.1	636.4	11.7
28(RS)	1.190	.841	125.2	70.14	18.7	0	14.1	575.7	13.4
29(SR)	1.201	.906	135.7	70.09	26.5	0	13.9	573.8	13.2
30(RS)	1.311	.795	156.9	90.11	22.5	0	13.6	605.5	12.5
31(RS)	1.383	.786	170.9	100.10	24.0	0	13.3	632.4	12.0
33	1.432	-	174.7	100.16	20.0	3.9	16.5	551.0	12.0
34	1.380	-	166.8	90.05	18.0	3.9	16.2	552.2	12.3
35	1.203	-	124.7	70.06	18.0	3.6	15.6	550.9	13.5
36	1.211	-	116.8	70.12	12.5	10.3	24.3	659.2	13.6
37	1.386	-	166.5	90.16	18.5	11.0	25.8	671.9	12.2
38	1.463	-	171.5	100.28	15.5	11.0	25.9	673.2	12.1
39	1.445	-	173.1	100.22	17.0	7.4	19.7	610.3	12.1
40	1.384	-	166.1	90.13	17.0	7.0	19.5	613.9	12.3
41	1.208	-	120.4	70.12	14.0	5.9	18.2	604.8	13.6
42	1.205	-	142.5	70.14	50.0	10.2	24.2	673.6	12.9
43	1.208	-	132.1	70.14	23.0	10.0	24.1	674.9	13.2
44	1.210	-	126.0	70.06	18.0	9.9	24.0	675.4	13.4
45*	1.210	-	119.4	70.09	14.0	9.9	23.9	676.0	13.5
46	1.330	-	176.4	90.11	50.0	10.1	25.8	679.1	11.7
47	1.370	-	171.9	90.11	25.0	10.1	25.7	679.8	12.0
48*	1.378	-	171.0	90.13	22.0	10.1	25.6	679.8	12.0
49*	1.384	-	168.8	90.14	20.0	10.0	25.5	680.1	12.1
50	1.376	-	181.9	100.16	50.0	10.1	26.2	679.8	11.5

*Data points not appearing in figure 11.
(RS) indicates a rotating-stall overall performance reading.
(SR) indicates a stall-removal overall performance reading.

Table 3 (c). (Continued)

Rdg.	Total Pressure Ratio	Rotor Adiabatic Efficiency	Inlet Corrected Flow, lbs/sec	Corrected Speed, % Design	Throttle Valve Setting	Blowing Corrected Flow lbs/sec	Blowing Air Plenum P, psia	Blowing Air Plenum T, °R	Plane 0.9 Casing Static p, psia
51	1.432	-	177.5	100.20	22.0	9.8	26.1	680.2	11.8
52	1.443	-	175.2	100.18	19.0	9.9	25.9	680.1	11.9
53*	1.454	-	173.6	100.22	17.0	9.9	25.8	680.8	12.0
54(RS)	1.379	-	163.3	90.16	17.3	9.2	25.3	680.5	12.4
55(SR)	1.385	-	168.8	90.17	19.3	9.3	25.5	681.9	12.1
56(RS)	1.459	-	170.6	100.17	14.3	9.3	25.1	682.8	12.2
57(SR)	1.466	-	171.7	100.20	14.8	9.4	25.8	682.4	12.2
58	1.405	.826	178.8	100.11	29.0	0	13.3	659.2	11.7

Table 3 (d). - Overall Performance for Circumferential Inlet Distortion Testing.

59	1.192	.742	105.7	70.05	6.0	0	14.6	571.5	13.8
60	1.170	.840	138.8	70.12	50.0	0	13.6	555.4	13.2
61	1.284	.854	169.8	90.10	50.0	0	12.9	574.4	12.3
62	1.327	.734	136.2	90.03	7.0	0	14.3	589.2	13.1
63	1.345	.759	177.9	100.07	50.0	0	12.4	601.2	12.0
64	1.408	.720	150.0	100.04	7.5	0	14.2	617.8	12.7
65	1.193	-	99.9	70.10	5.0	2.9	15.8	558.3	14.0
66	1.330	-	134.9	90.11	7.5	3.4	16.1	556.4	13.1
67	1.412	-	148.2	100.12	7.5	3.2	16.2	554.2	12.8
68	1.410	-	139.6	100.11	7.5	9.9	24.4	681.7	13.1
69	1.326	-	122.7	90.14	6.5	9.7	23.5	664.7	13.5
70	1.194	-	88.0	70.13	3.5	7.8	23.0	664.4	14.1
71	1.195	-	93.1	70.18	4.0	5.8	18.2	605.1	14.1
72	1.328	-	129.3	90.29	7.0	6.2	18.8	609.4	13.4
73	1.415	-	142.9	100.27	7.0	6.5	19.3	622.9	13.0
74(RS)	1.402	-	134.5	100.19	5.7	8.6	23.7	691.4	13.3
75(SR)	1.408	-	139.7	100.14	7.3	8.9	24.1	694.7	13.1
76(RS)	1.321	-	118.1	90.17	5.0	8.4	23.4	678.9	13.6
77(SR)	1.327	-	128.7	90.18	8.0	8.5	23.6	677.7	13.4
78(RS)	1.194	-	85.3	70.18	2.8	8.5	23.1	675.9	14.1
79(SR)	1.195	-	89.7	70.20	4.3	8.3	23.0	676.3	14.1

*Data points not appearing in figure 11.
(RS) indicates a rotating-stall overall performance reading.
(SR) indicates a stall removal overall performance reading.

Table 3 (d). (Continued)

Rdg.	Total Pressure Ratio	Rotor Adiabatic Efficiency	Inlet Corrected Flow lbs/sec	Corrected Speed % Design	Throttle Valve Setting	Blowing Corrected Flow lbs/sec	Blowing Air Plenum P, psia	Blowing Air Plenum T, °R	Plane 0.9 Casing Static p, psia
80(RS)	1.174	.698	97.5	70.23	4.6	0	14.9	615.9	14.0
81(SR)	1.193	.743	104.0	70.19	5.4	0	14.7	601.1	13.9
82(RS)	1.298	.694	128.2	90.25	5.7	0	14.9	627.9	13.4
83(SR)	1.328	.731	134.8	90.26	6.7	0	14.4	605.6	13.1
84(RS)	1.366	.674	136.7	100.34	5.5	0	14.9	648.7	13.2
85(SR)	1.407	.717	148.6	100.21	7.2	0	14.3	630.1	12.7
86	1.398	.728	157.5	100.28	10.0	0	13.9	628.6	12.6
87	1.392	.749	163.3	100.24	12.5	0	13.6	626.8	12.4
88	1.374	.752	170.5	100.24	18.0	0	13.2	622.7	12.3
89	1.312	.786	159.9	90.29	17.0	0	13.4	595.5	12.5
90	1.412	-	148.0	100.26	7.5	8.9	24.2	682.7	12.9
91	1.406	-	157.1	100.22	12.0	8.9	24.3	682.7	12.7
92	1.387	-	168.7	100.22	18.0	9.0	24.4	680.0	12.4
93	1.344	-	177.4	100.23	50.0	9.0	24.5	680.9	12.1
94	1.326	-	133.1	90.13	9.5	8.9	24.0	661.5	13.3
95	1.330	-	142.4	90.15	12.0	9.0	24.1	662.0	13.0
96	1.320	-	155.6	90.12	18.0	9.1	24.2	661.8	12.7
97	1.288	-	167.8	90.19	50.0	9.2	24.2	661.5	12.4
98	1.192	-	97.8	70.14	7.0	8.5	23.3	661.1	13.9
99	1.189	-	111.3	70.13	11.0	8.6	23.3	661.6	13.7
100	1.187	-	123.6	70.14	17.0	8.7	23.4	661.6	13.5
101	1.170	-	138.7	70.13	50.0	8.8	23.5	662.7	13.2
102	1.179	.836	129.8	70.09	20.0	0	13.9	578.0	13.4
103	1.188	.804	119.9	70.13	12.0	0	14.2	576.4	13.6
104	1.192	.783	112.1	70.08	8.0	0	14.4	575.7	13.7
105	1.311	.794	159.5	90.13	17.0	0	13.4	580.6	12.6
106	1.321	.776	150.8	90.10	12.0	0	13.8	582.4	12.7
107	1.327	.759	143.3	90.14	9.0	0	14.1	586.5	12.9

(RS) indicates a rotating-stall overall performance reading.
(SR) indicates a stall-removal overall performance reading.

Table 3 (e). - Overall Performance for Complete Undistorted Inlet Testing.

Rdg.	Total Pressure Ratio	Rotor Adiabatic Efficiency	Inlet Corrected Flow, lbs/sec	Corrected Speed, % Design	Throttle Valve Setting	Blowing Corrected Flow lbs/sec	Blowing Air Plenum P, psia	Blowing Air Plenum T, °R	Plane 0.9 Casing Static p, psia
108	1.365	.885	162.8	90.15	7.0	0	13.6	584.2	12.8
109	1.469	.859	174.4	100.27	6.3	0	13.7	607.0	12.5
110	1.469	-	174.0	100.12	8.4	8.9	23.4	650.2	12.7
111	1.367	-	163.5	90.31	9.4	9.0	23.3	651.5	13.0
112	1.206	-	120.4	70.15	8.3	8.8	23.0	647.7	13.7
113(RS)	1.200	-	112.8	70.14	7.3	8.9	23.2	649.4	13.8
114(SR)	1.204	-	118.2	70.14	7.8	8.8	23.2	650.1	13.8
115(RS)	1.362	-	153.0	90.20	8.2	8.9	23.3	651.0	13.2
116(SR)	1.374	-	158.2	90.14	8.6	8.9	23.4	651.7	13.1
117(RS)	1.466	-	165.3	100.15	7.3	8.9	23.5	654.0	12.9
119(RS)	1.455	.830	164.7	100.08	5.3	0	14.0	640.3	12.8
120(SR)	1.467	.866	175.1	100.10	6.3	0	13.8	634.1	12.5
121(RS)	1.357	.856	154.3	90.13	6.0	0	13.9	609.7	13.0
122(SR)	1.371	.886	159.1	90.22	6.4	0	13.8	610.0	12.8
123(RS)	1.200	.831	115.9	70.13	5.0	0	14.3	583.9	13.8
124(SR)	1.204	.860	119.5	70.19	5.3	0	14.3	580.2	13.7
125	1.203	.879	124.1	70.20	6.2	0	14.2	576.4	13.7
126	1.177	-	143.8	70.23	19.0	8.8	22.8	655.6	13.4
127	1.187	-	138.6	70.17	15.0	8.8	22.9	656.9	13.5
129	1.197	-	131.2	70.19	11.0	8.8	23.1	663.1	13.6
130	1.139	-	157.2	70.18	50.0	8.9	22.7	662.9	13.1
131	1.282	-	177.8	90.27	19.0	8.9	22.8	658.7	12.7
132	1.316	-	174.6	90.21	14.0	8.9	23.1	658.0	12.7
133	1.350	-	168.5	90.26	10.5	9.0	23.2	657.8	12.9
134	1.205	-	180.1	90.28	50.0	8.9	22.7	657.9	12.6
135	1.357	-	185.3	100.29	15.0	9.0	22.9	659.7	12.4
136	1.395	-	183.8	100.29	12.0	9.0	23.2	660.0	12.5
137	1.437	-	180.2	100.30	10.0	9.0	23.4	660.4	12.5
138(SR)	1.484	-	170.0	100.33	7.6	9.0	23.6	661.2	12.8
139	1.235	-	186.7	100.30	50.0	9.0	22.9	658.9	12.4
140	1.234	.725	190.9	100.31	50.0	0	11.2	572.6	11.9

(RS) indicates a rotating-stall overall performance reading.
(SR) indicates a stall-removal overall performance reading.

Table 3 (e). (Continued)

Rdg.	Total Pressure Ratio	Rotor Adiabatic Efficiency	Inlet Corrected Flow, lbs/sec	Corrected Speed, % Design	Throttle Valve Setting	Blowing Corrected Flow lbs/sec	Blowing Air Plenum P, psia	Blowing Air Plenum T, °R	Plane 0.9 Casing Static p, psia
141	1.329	.803	190.6	100.37	15.0	0	12.1	594.1	12.0
142	1.392	.843	186.8	100.38	10.0	0	12.7	593.1	12.2
143	1.432	.861	182.4	100.38	8.0	0	13.2	601.0	12.3
144	1.336	.893	172.5	90.27	8.8	0	13.2	587.7	12.6
145	1.307	.881	178.1	90.26	12.0	0	12.8	581.4	12.4
146	1.263	.842	183.2	90.30	19.0	0	12.1	579.5	12.3
147	1.208	.771	184.2	90.29	50.0	0	11.6	554.6	12.2
148	1.142	.864	161.0	70.24	50.0	0	12.8	561.8	12.9
149	1.170	.890	148.1	70.23	17.0	0	13.4	563.5	13.2
150	1.184	.892	141.2	70.24	12.0	0	13.7	560.3	13.3
151	1.194	.887	133.3	70.22	8.5	0	13.9	561.0	13.5

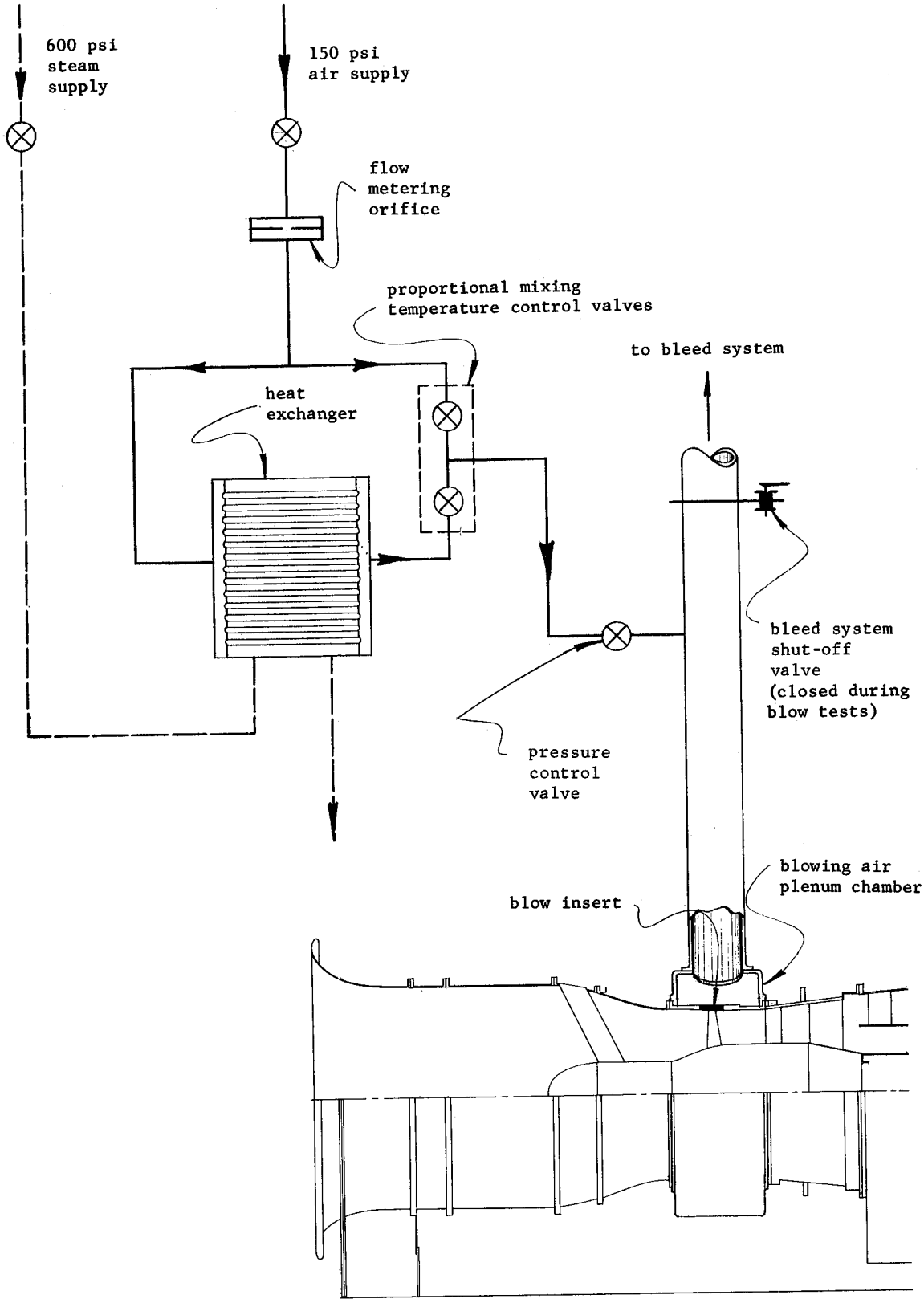

Figure 1. - Schematic diagram of blowing air system.

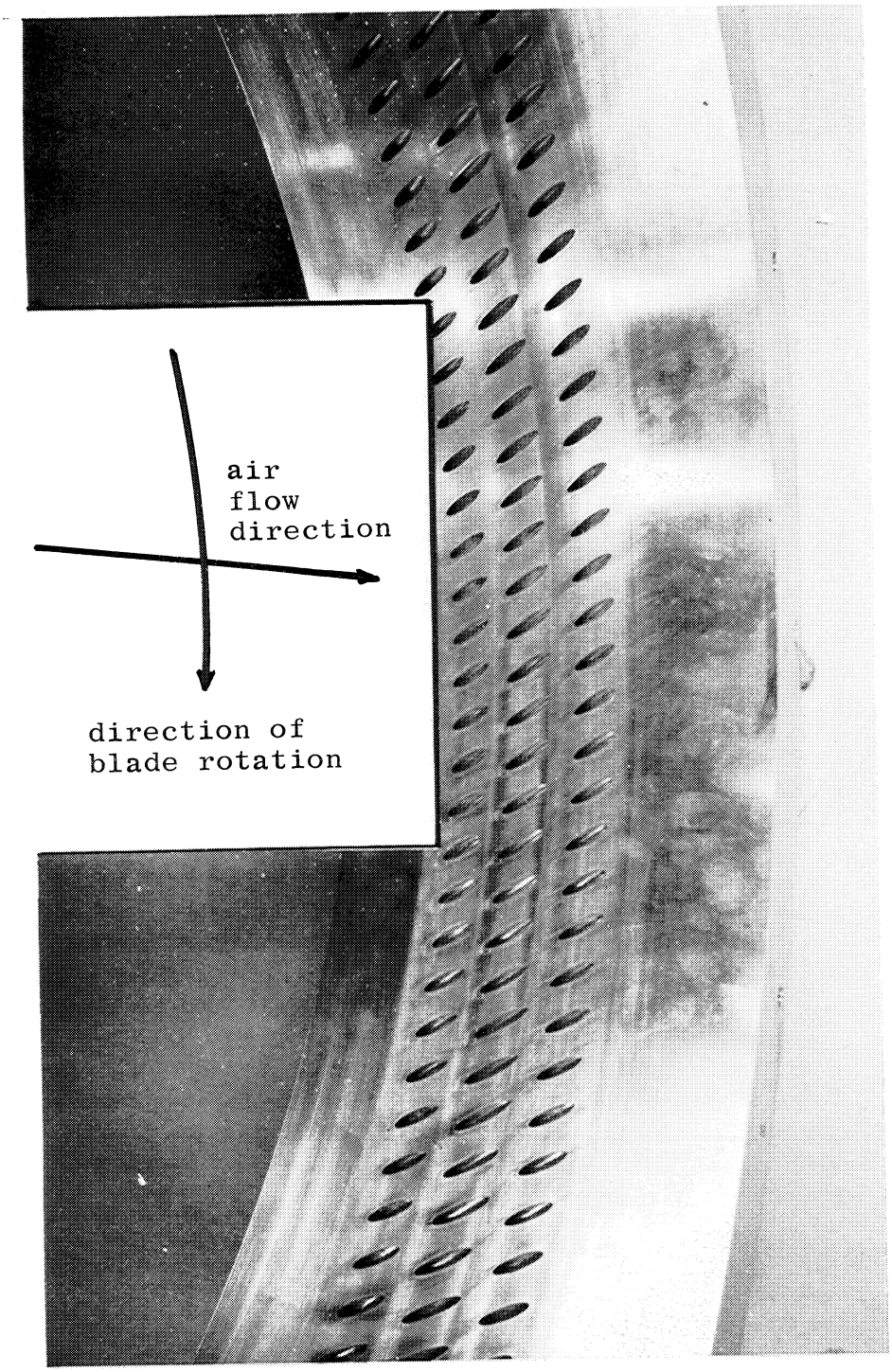

Figure 2. - View of blowing insert configuration no. 1

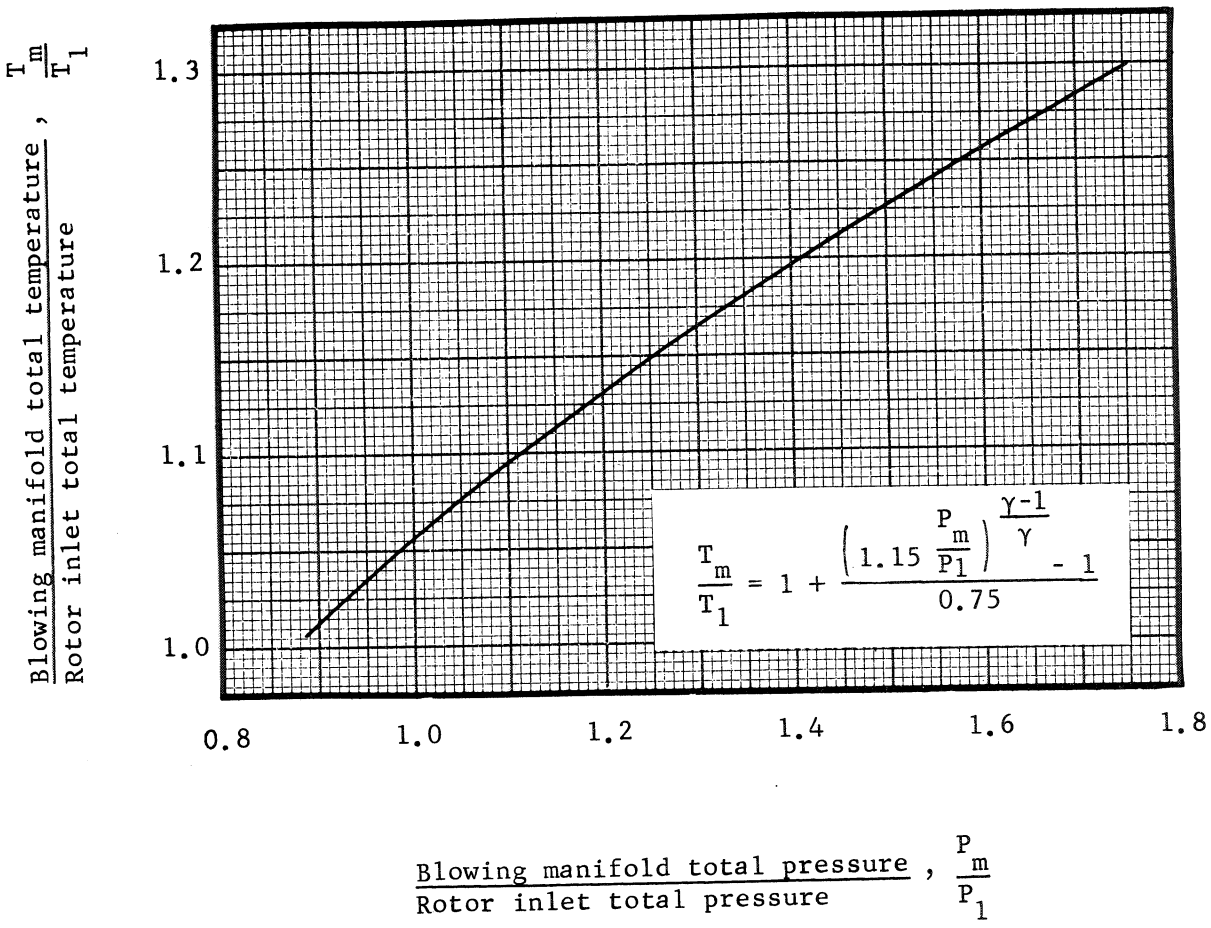

Figure 3 . - Blowing manifold temperature-pressure relation.

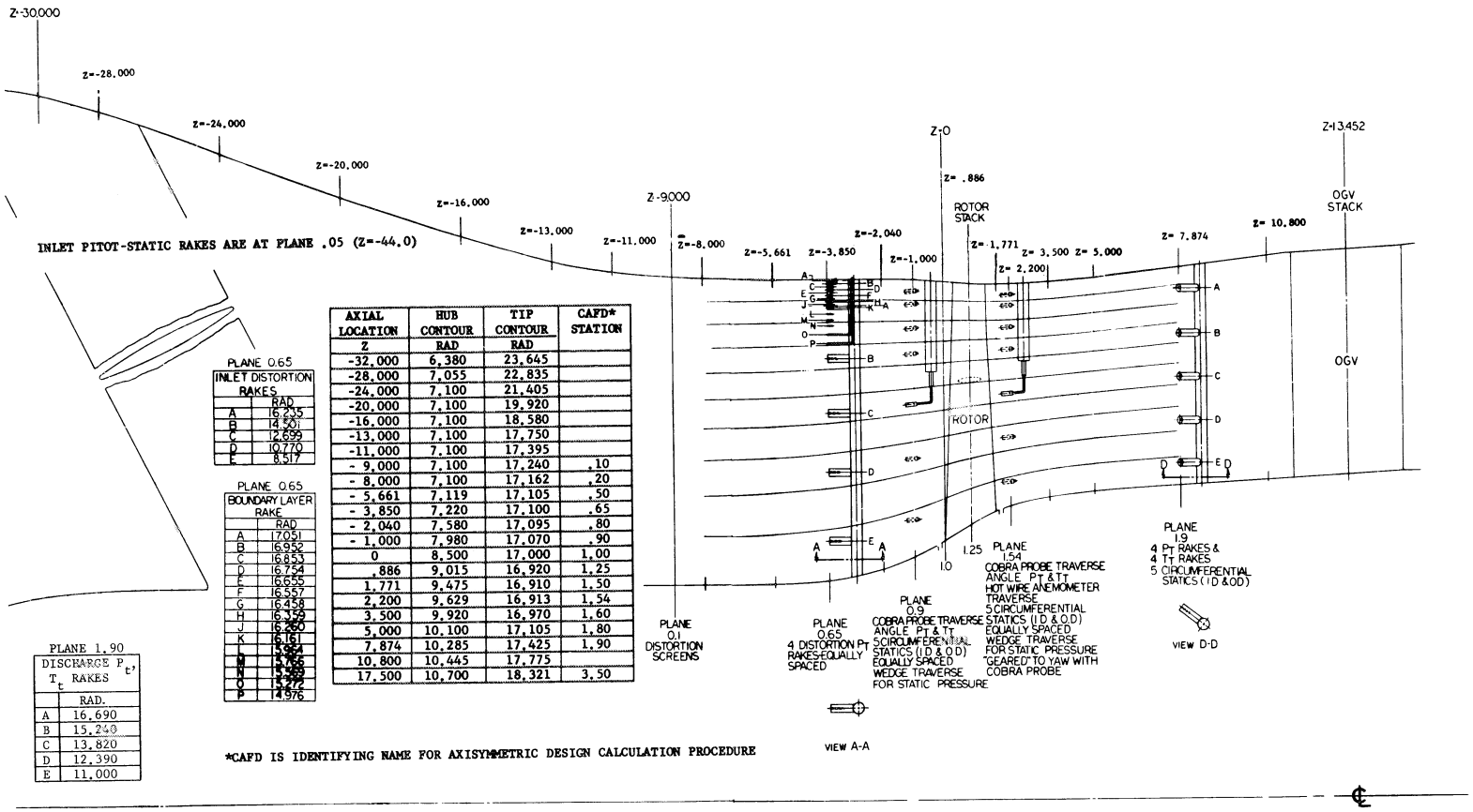

PLANE 0.65
INLET DISTORTION RAKES

	RAD
A	16.235
B	14.561
C	12.899
D	10.770
E	8.517

PLANE 0.65
BOUNDARY LAYER RAKE

	RAD
A	17.051
B	16.952
C	16.853
D	16.754
E	16.655
F	16.557
G	16.458
H	16.359
J	16.260
K	16.161
L	15.964
M	15.766
N	15.568
O	15.372
P	14.976

AXIAL LOCATION Z	HUB CONTOUR RAD	TIP CONTOUR RAD	CAFD* STATION
-32.000	6.380	23.645	
-28.000	7.055	22.835	
-24.000	7.100	21.405	
-20.000	7.100	19.920	
-16.000	7.100	18.580	
-13.000	7.100	17.750	
-11.000	7.100	17.395	
- 9.000	7.100	17.240	.10
- 8.000	7.100	17.162	.20
- 5.661	7.119	17.105	.50
- 3.850	7.220	17.100	.65
- 2.040	7.580	17.095	.80
- 1.000	7.980	17.070	.90
0	8.500	17.000	1.00
.886	9.015	16.920	1.25
1.771	9.475	16.910	1.50
2.200	9.629	16.913	1.54
3.500	9.920	16.970	1.60
5.000	10.100	17.105	1.80
7.874	10.285	17.425	1.90
10.800	10.445	17.775	
17.500	10.700	18.321	3.50

PLANE 1.90
DISCHARGE P_t, T_t RAKES

	RAD.
A	16.690
B	15.240
C	13.820
D	12.390
E	11.000

*CAFD IS IDENTIFYING NAME FOR AXISYMMETRIC DESIGN CALCULATION PROCEDURE

Figure 4 - Meridional view showing location of instrumentation.

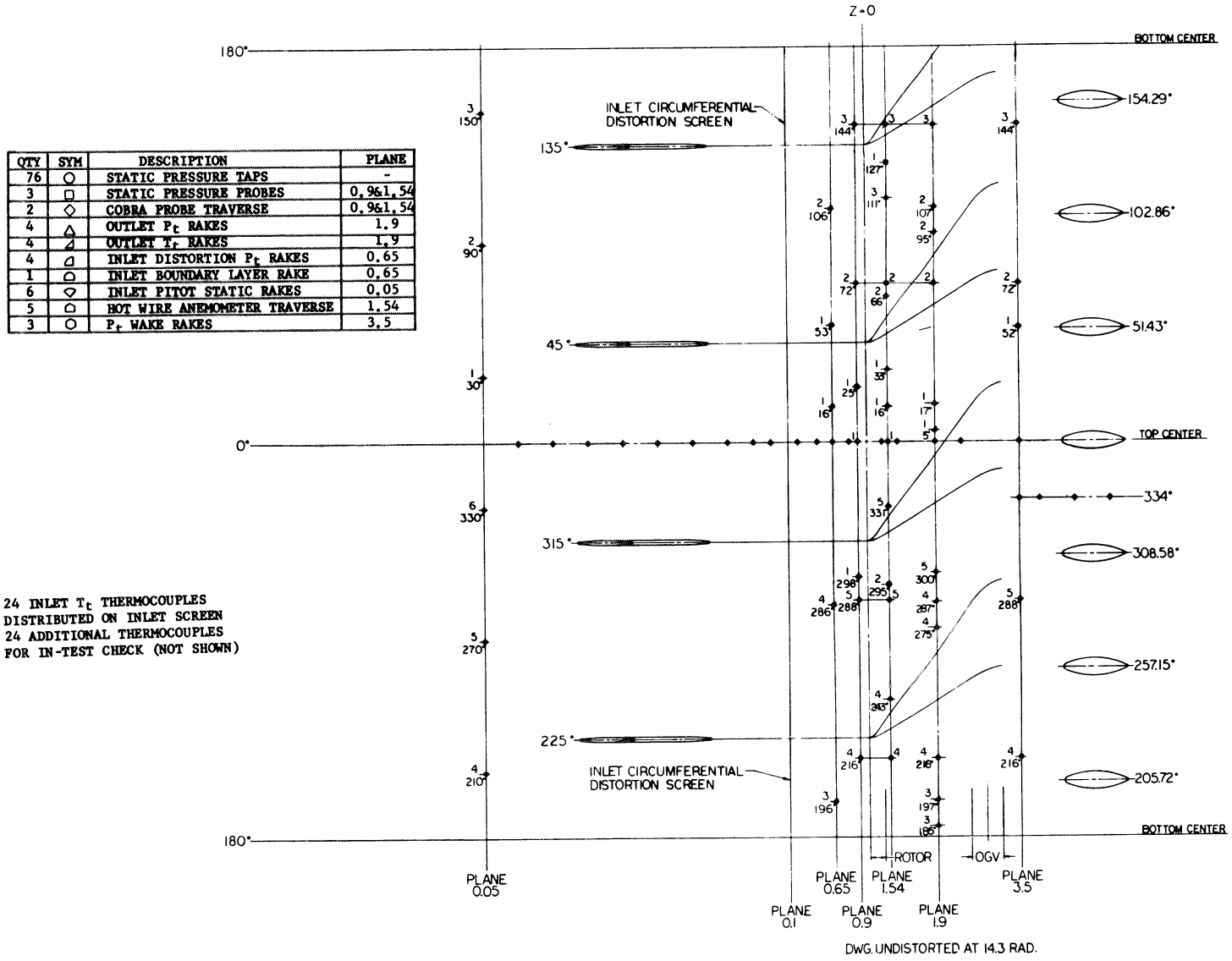

QTY	SYM	DESCRIPTION	PLANE
76	○	STATIC PRESSURE TAPS	-
3	□	STATIC PRESSURE PROBES	0, 9&1, 54
2	◇	COBRA PROBE TRAVERSE	0, 9&1, 54
4	△	OUTLET P_t RAKES	1, 9
4	◿	OUTLET T_t RAKES	1, 9
4	◭	INLET DISTORTION P_t RAKES	0.65
1	⌓	INLET BOUNDARY LAYER RAKE	0.65
6	▽	INLET PITOT STATIC RAKES	0, 05
5	⌓	HOT WIRE ANEMOMETER TRAVERSE	1, 54
3	○	P_t WAKE RAKES	3, 5

24 INLET T_t THERMOCOUPLES
DISTRIBUTED ON INLET SCREEN
24 ADDITIONAL THERMOCOUPLES
FOR IN-TEST CHECK (NOT SHOWN)

Figure 5 - Development Showing Circumferential Location of Instrumentation

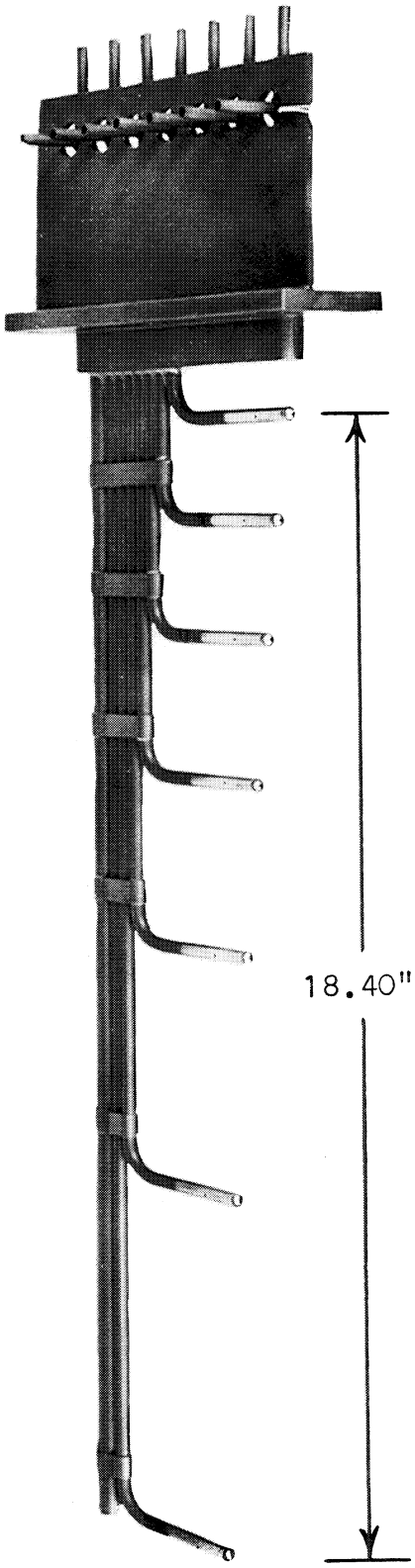

(a). - Inlet pitot-static rake.

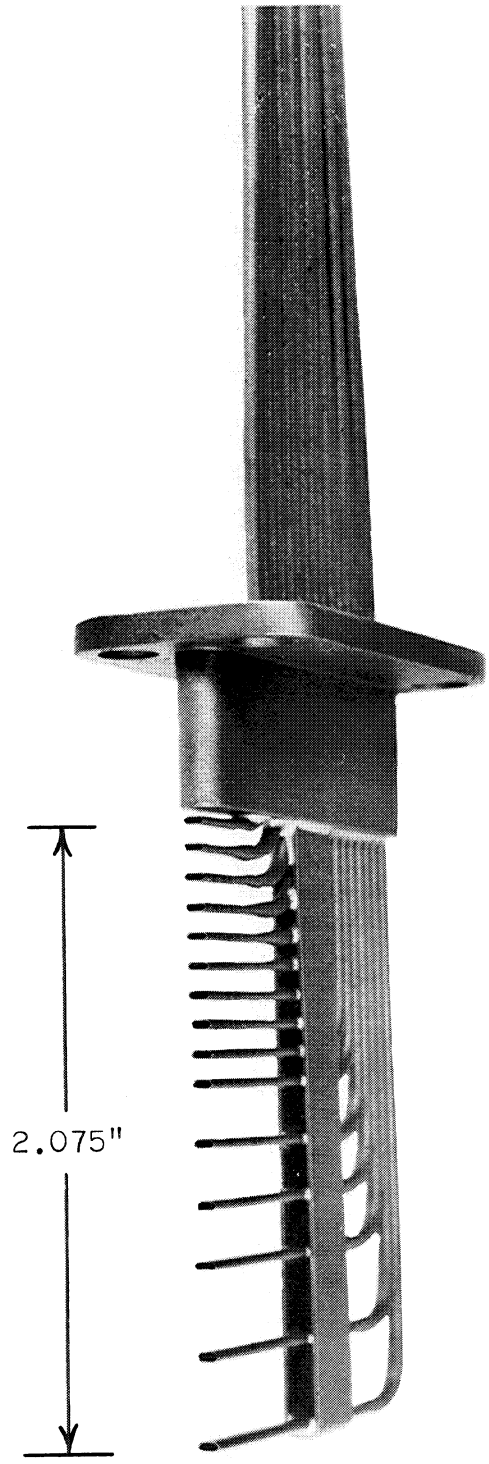

(b). - Casing boundary layer rake.

Figure 6 - Photographs of Instrumentation

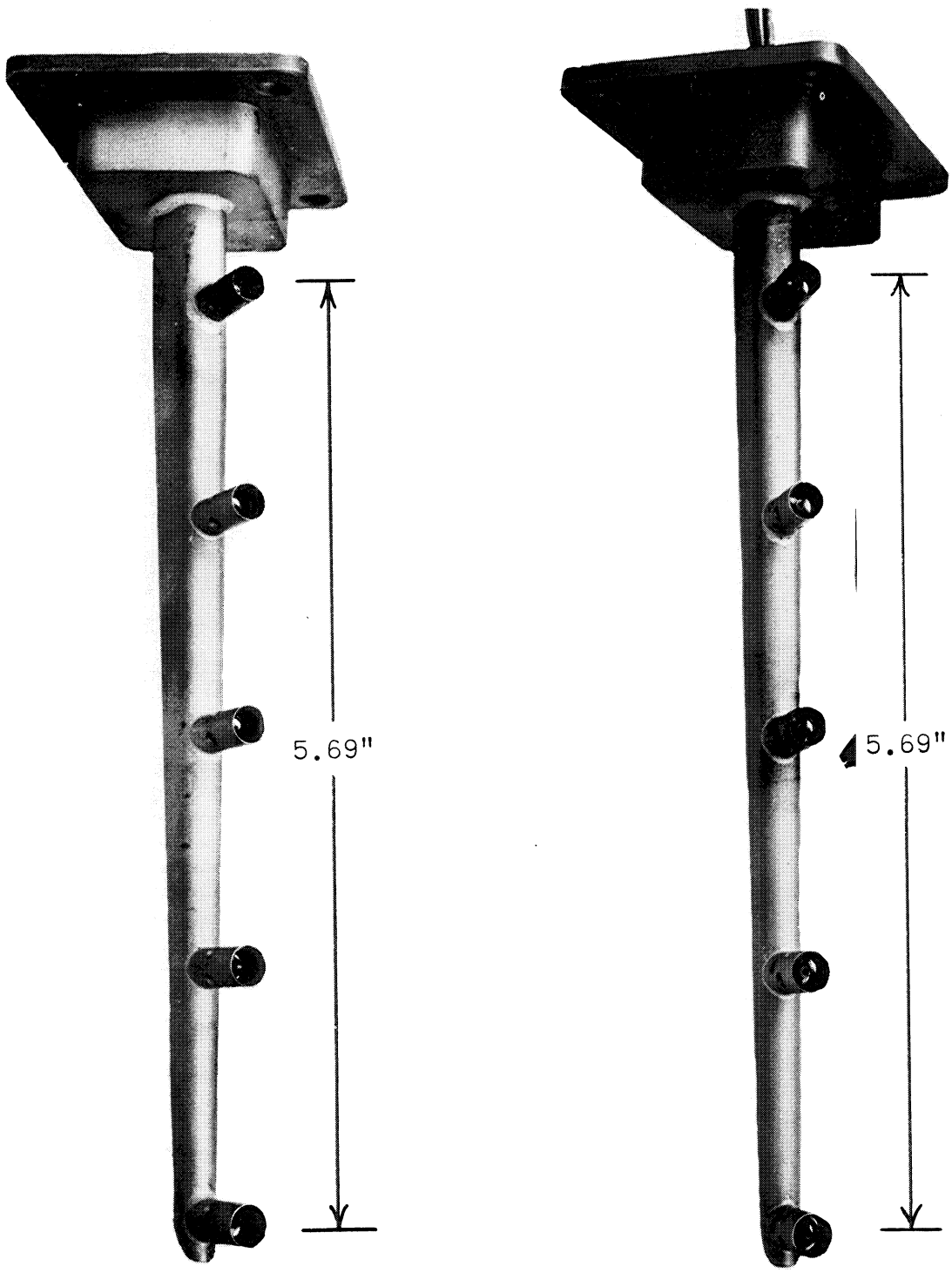

(c). - Discharge total temperature rake. (d). - Discharge total pressure rake.

Figure 6. - Photographs of instrumentation

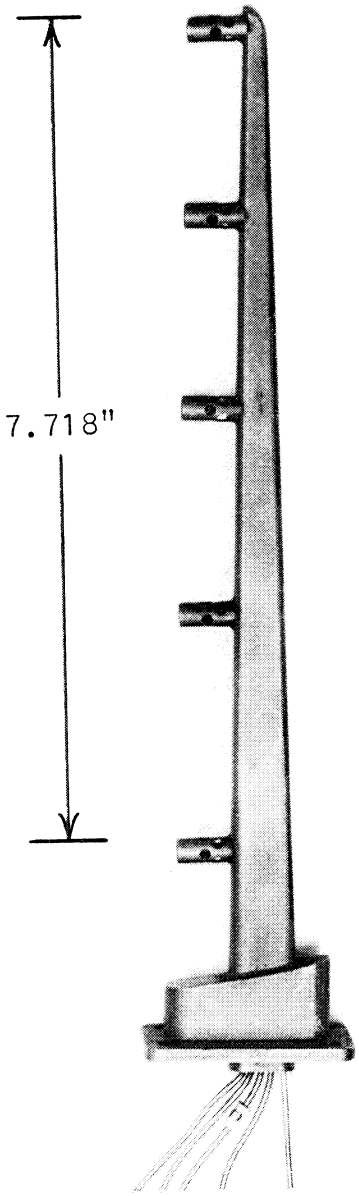

(e). - Inlet distortion total pressure rake.

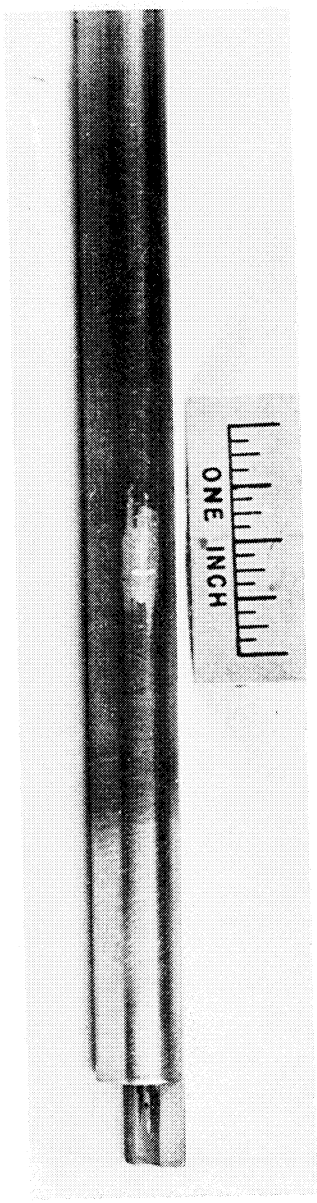

(f). - Shielded hot wire probe

Figure 6 - Photographs of Instrumentation

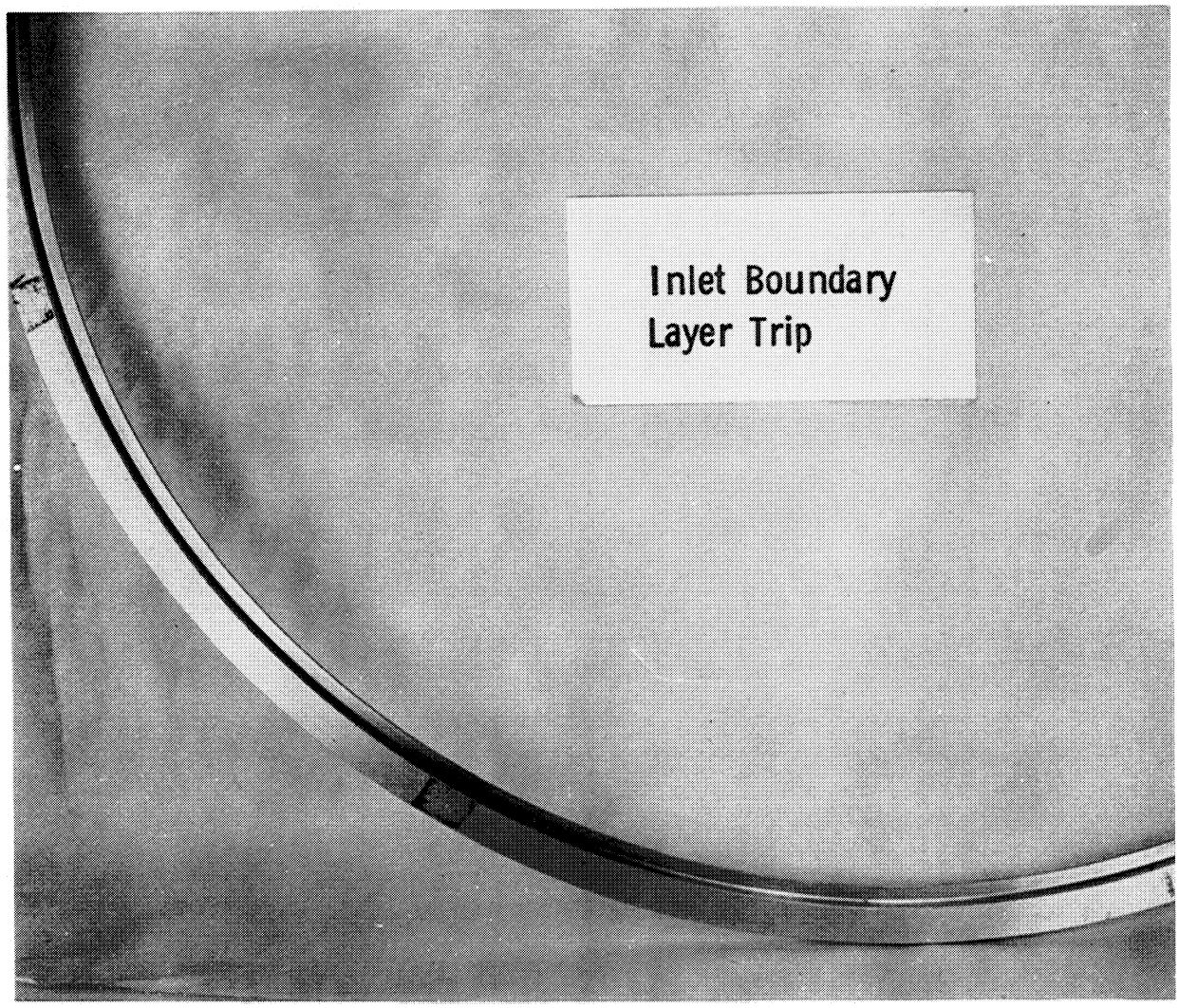

Figure 7(a) - Photograph of Inlet Boundary Layer Trip

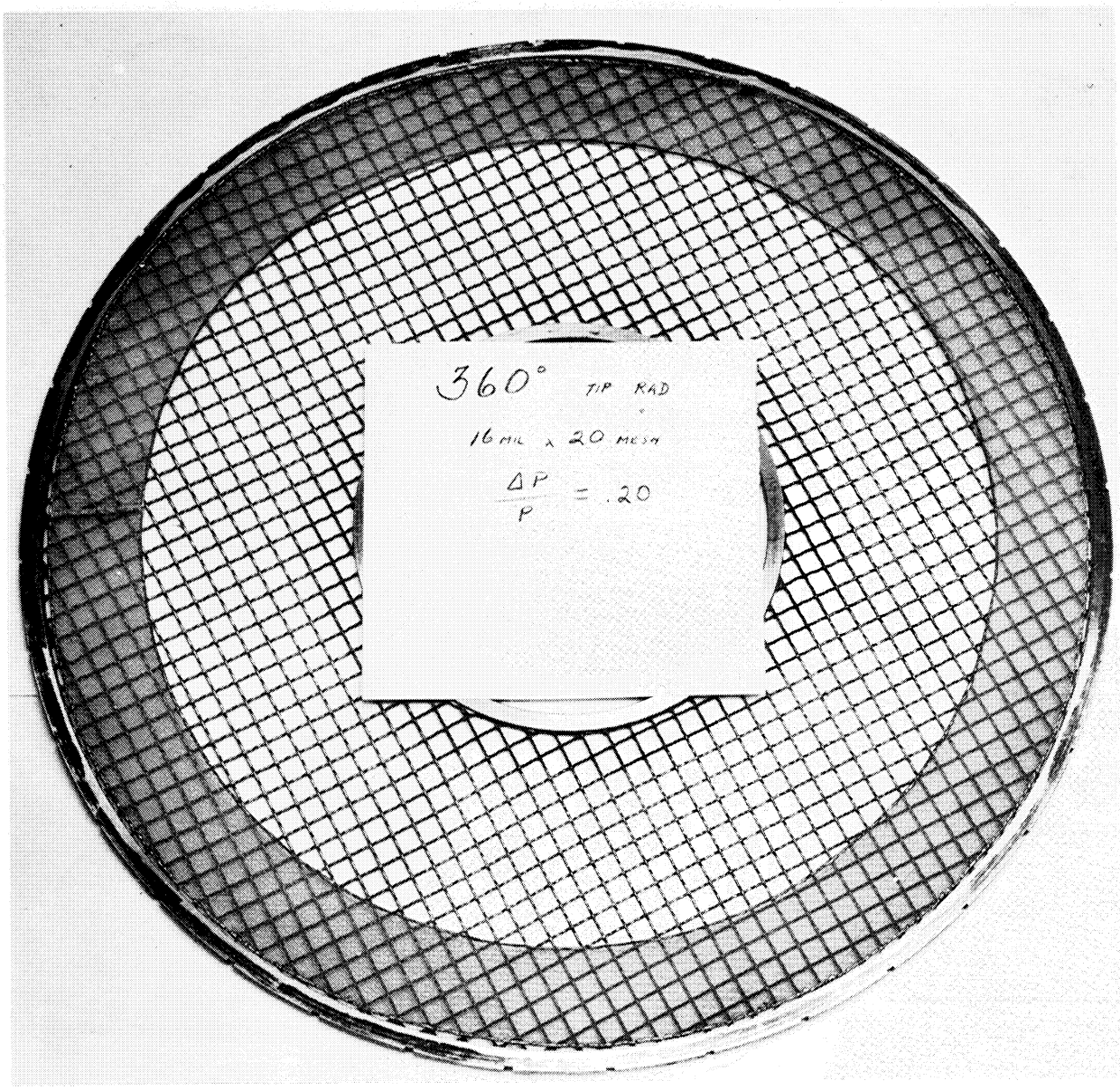

Figure 7(b) - Photograph of radial inlet distortion screen mounted on support screen.

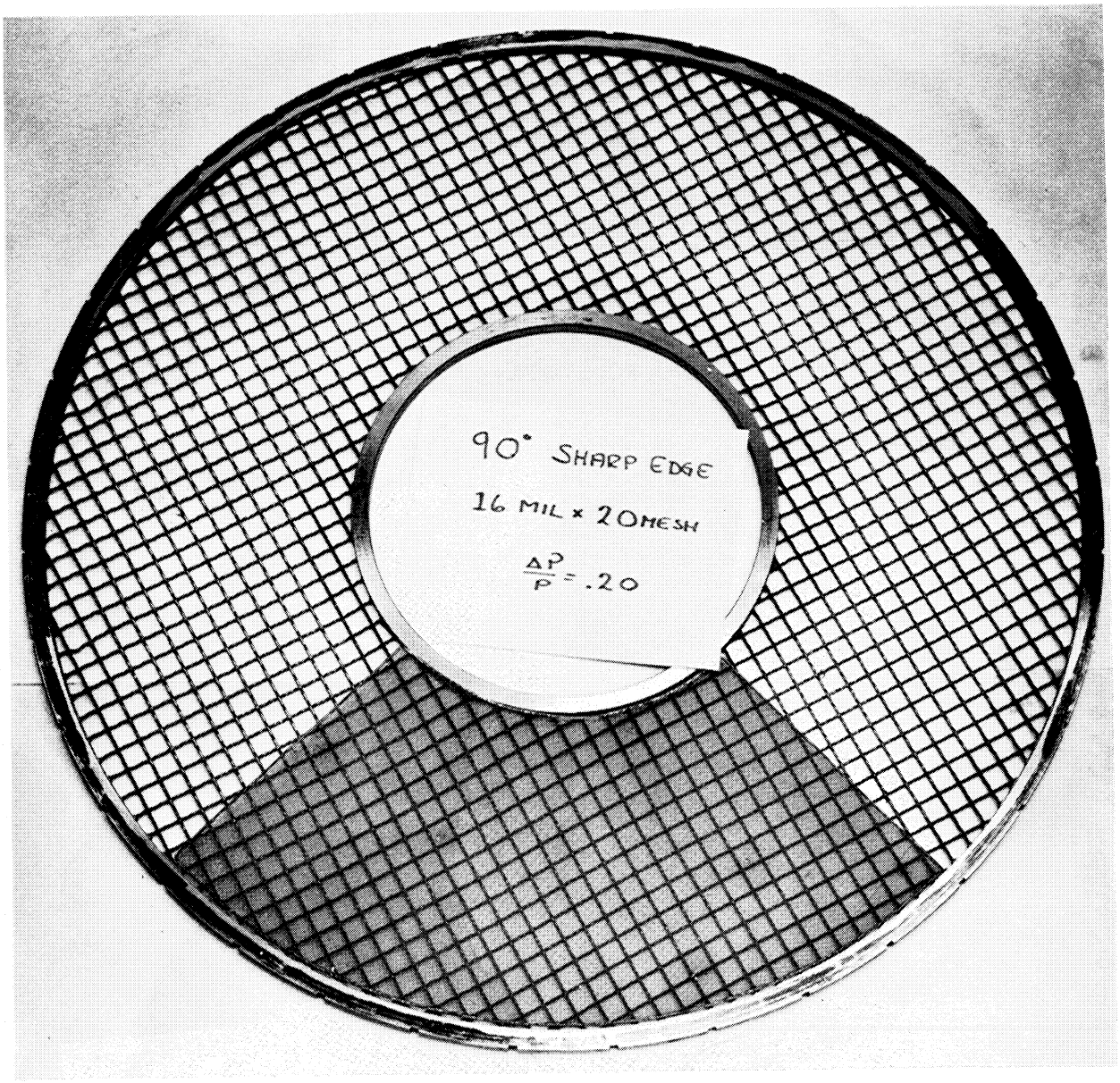

Figure 7(c). - Photograph of circumferential inlet distortion screen mounted on support screen.

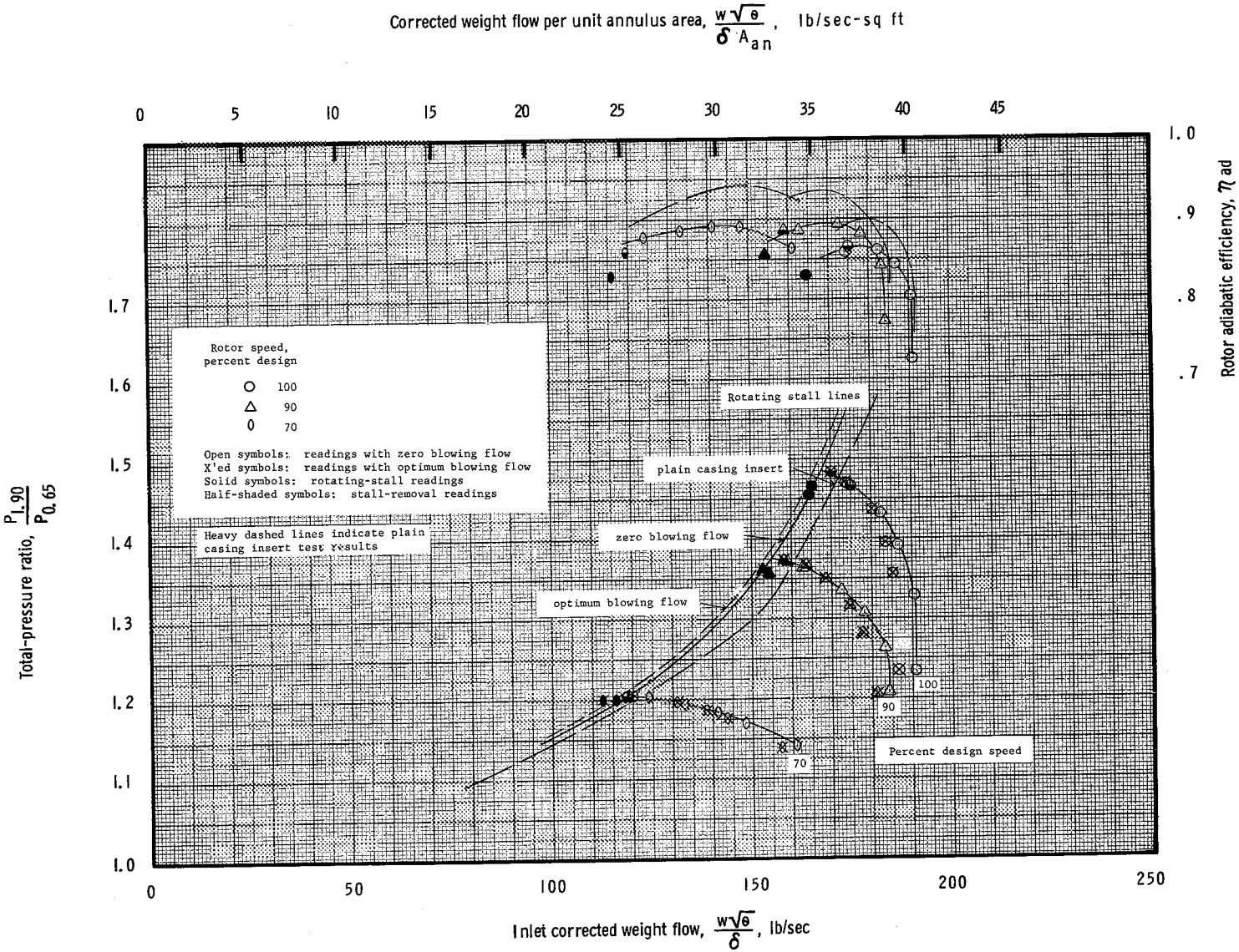

Figure 8. - Rotor performance map for undistorted inlet flow.

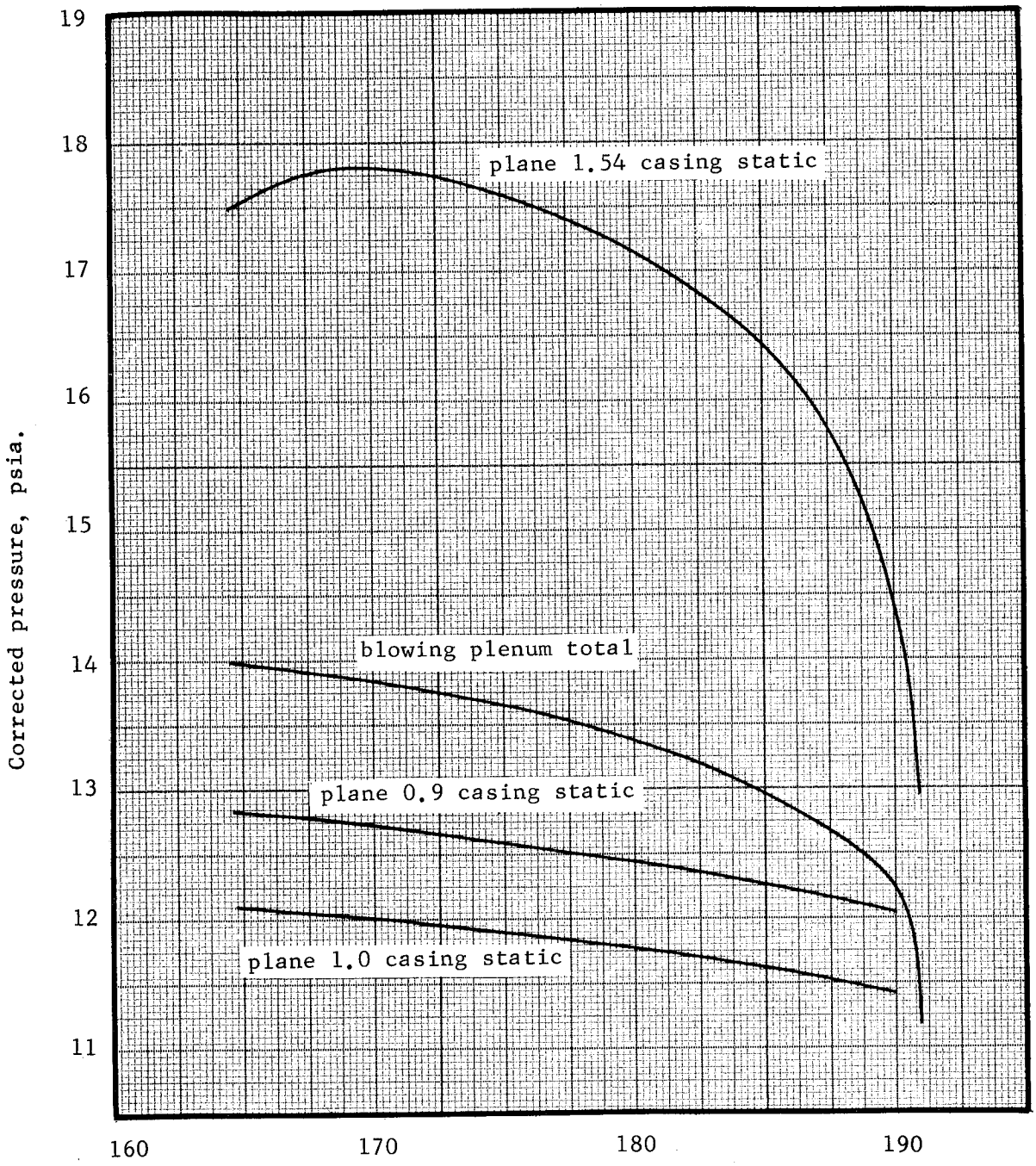

Figure 9. - Variation of blowing plenum pressure, at 100% design speed and zero blowing flow.

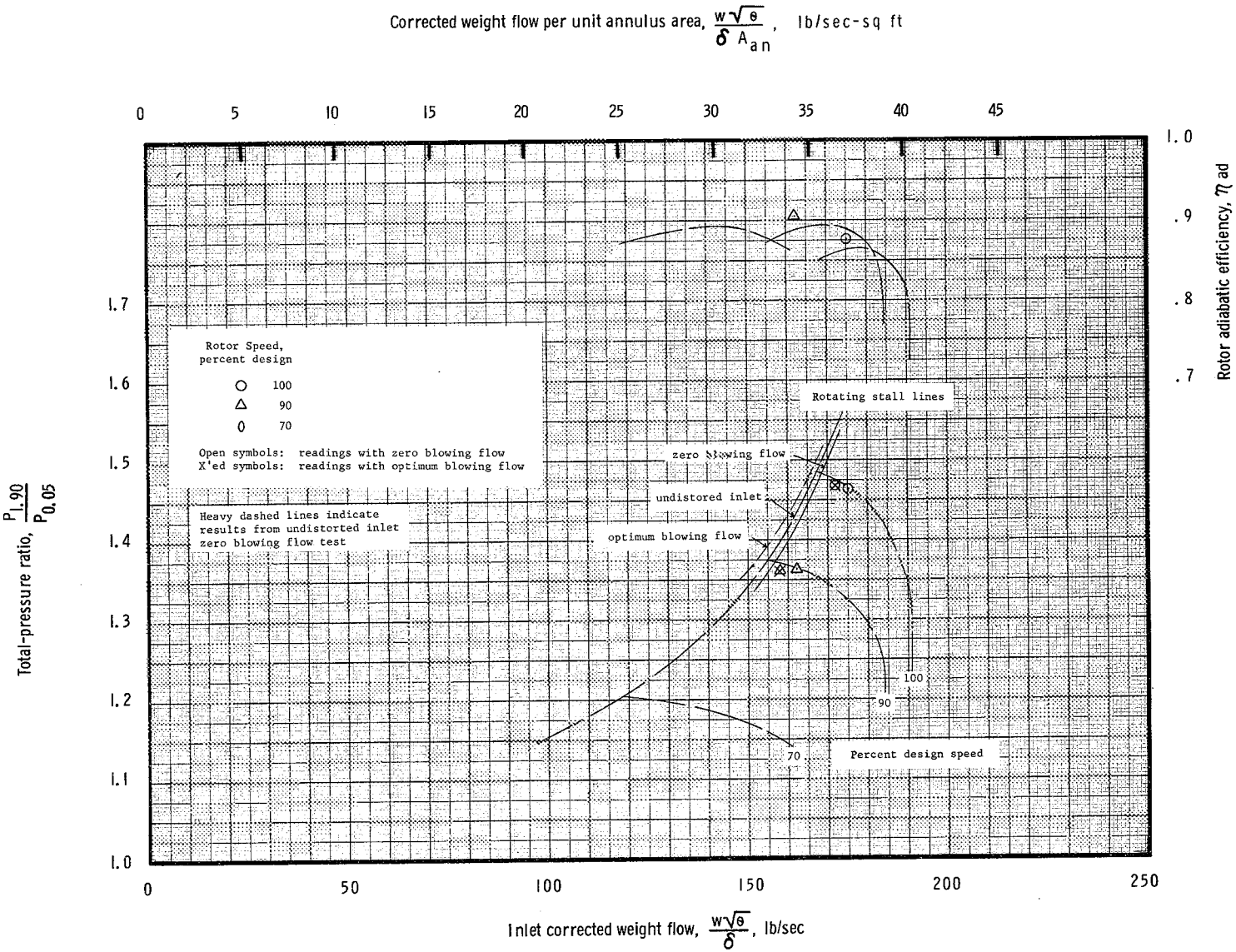

Figure 10. - Rotor performance map with boundary layer trip.

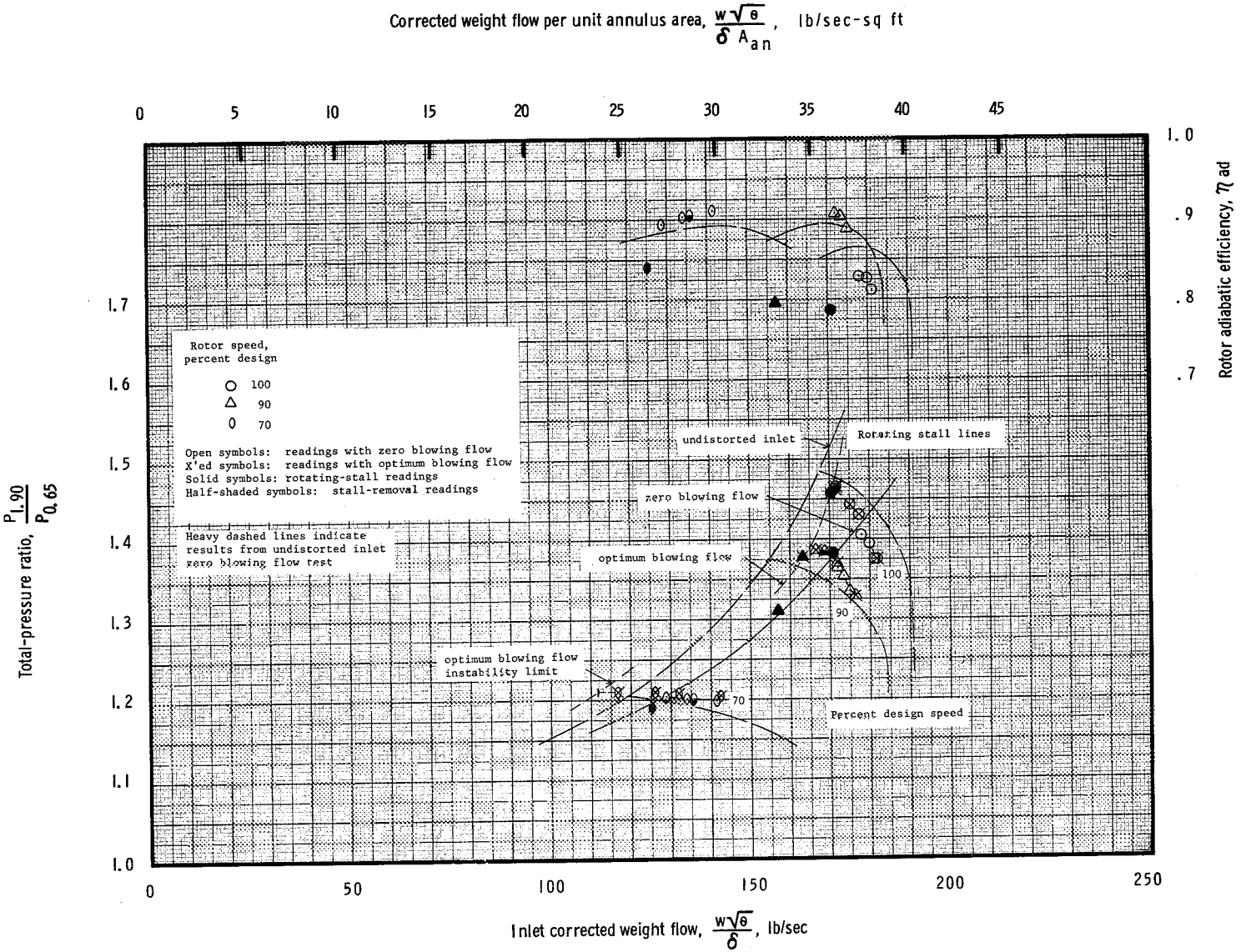

Figure 11. - Rotor performance map with radial inlet distortion.

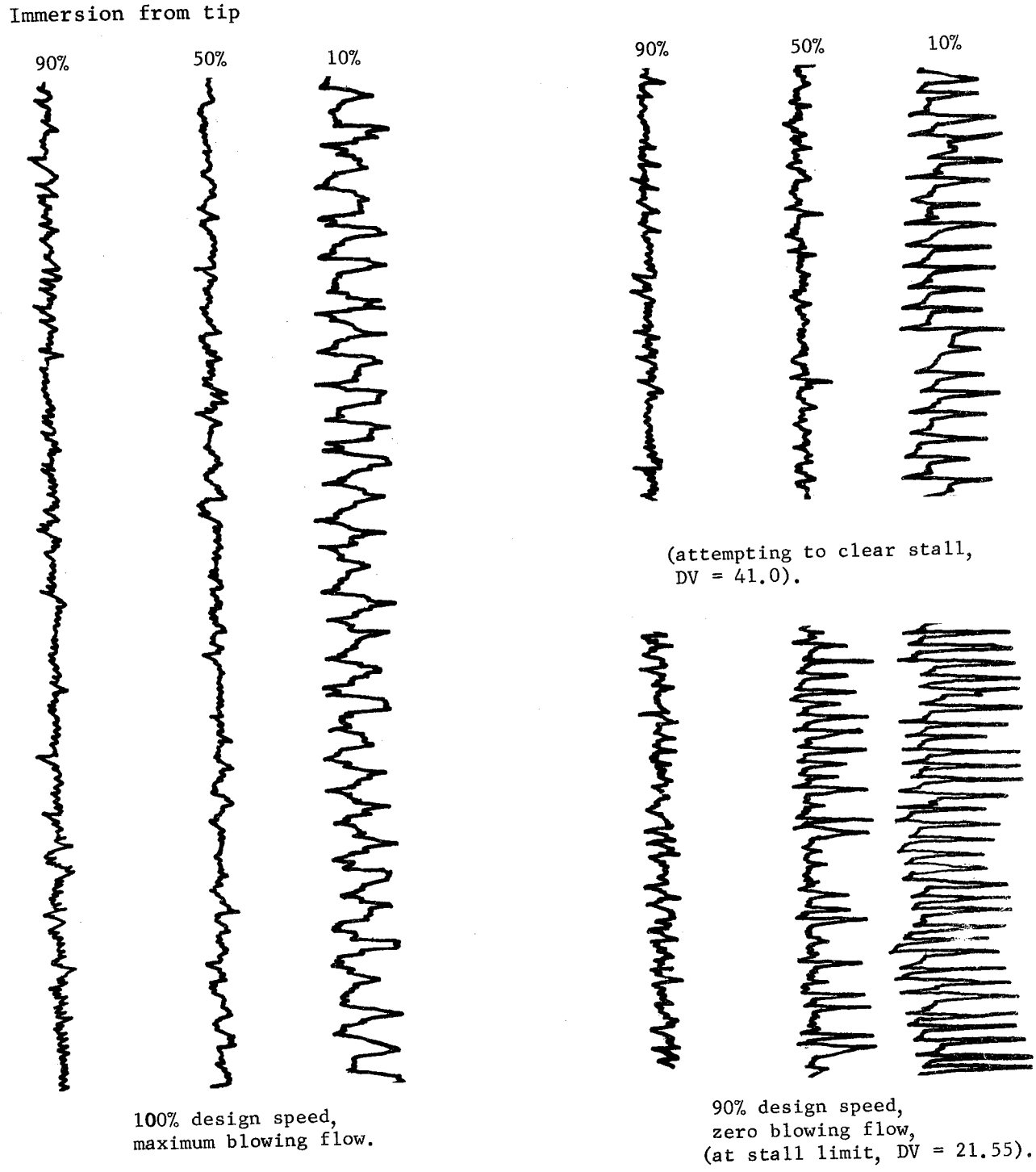

Figure 12. - Sample hot wire anemometer stall traces from radial distortion testing.

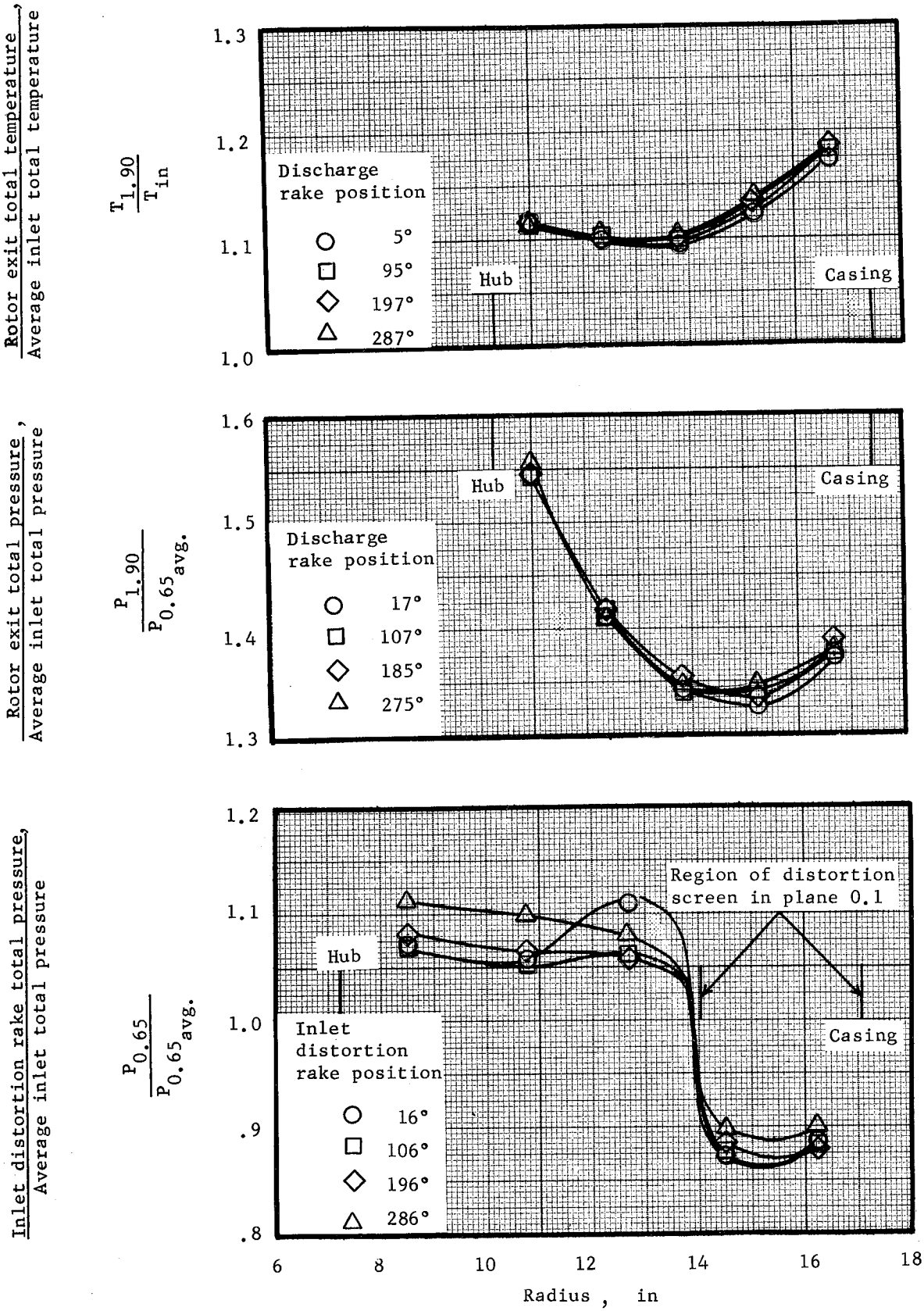

Figure 13 - Inlet total pressure exit total pressure and exit total temperature profiles at 100% design speed, with radial distortion, for Reading 16.

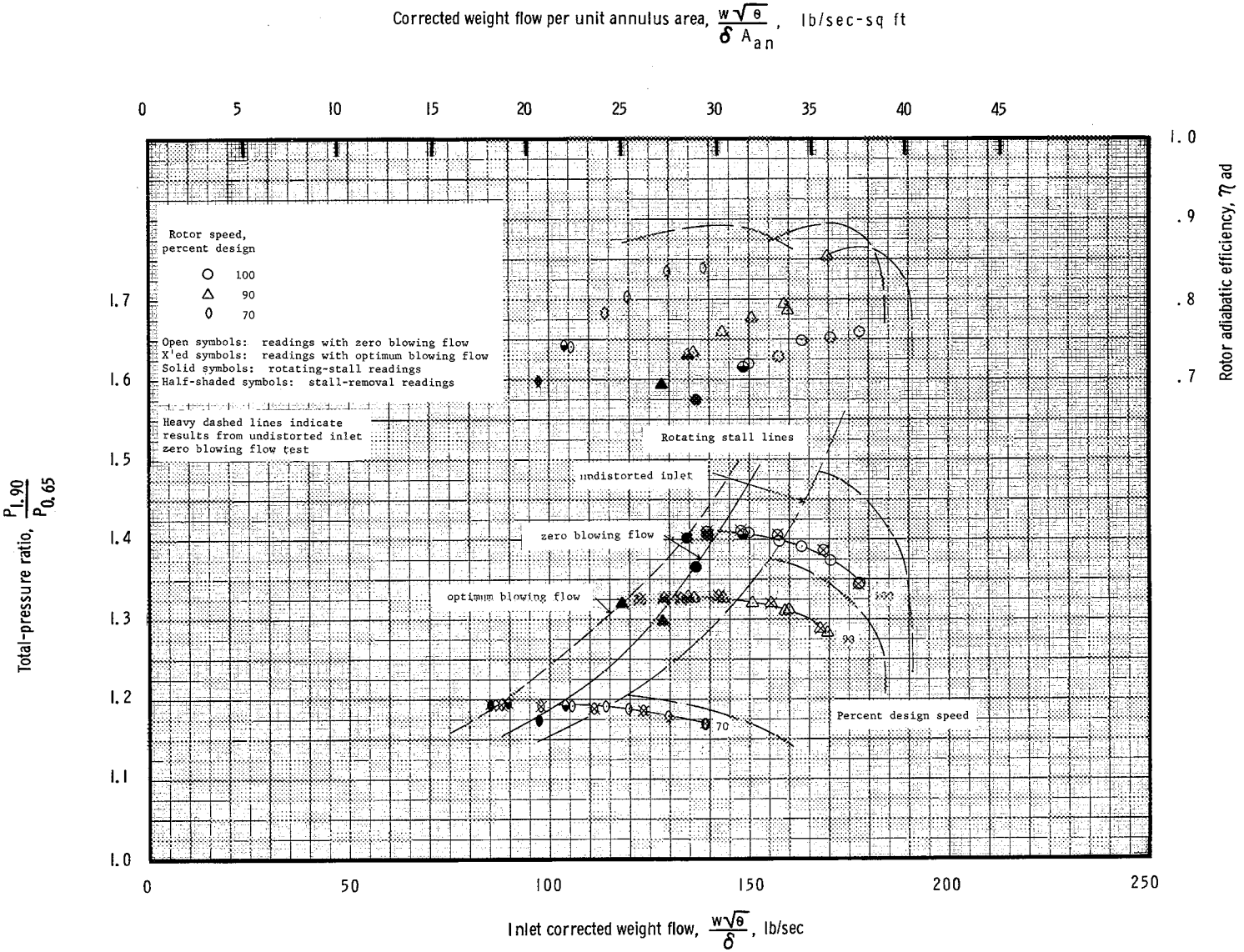

Figure 14. - Rotor performance map with circumferential inlet distortion.

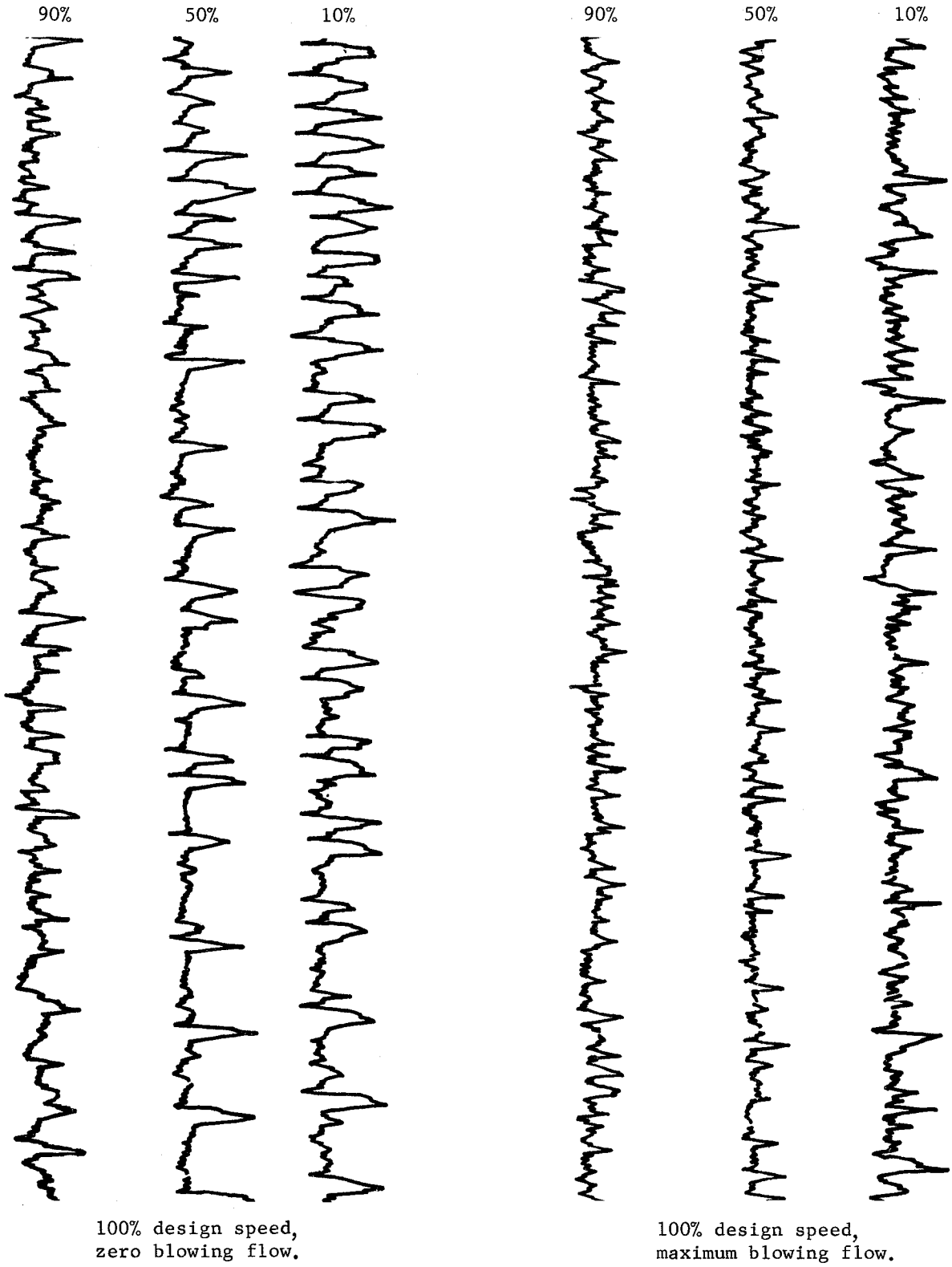

Figure 15. - Sample hot wire anemometer stall traces from circumferential distortion testing.

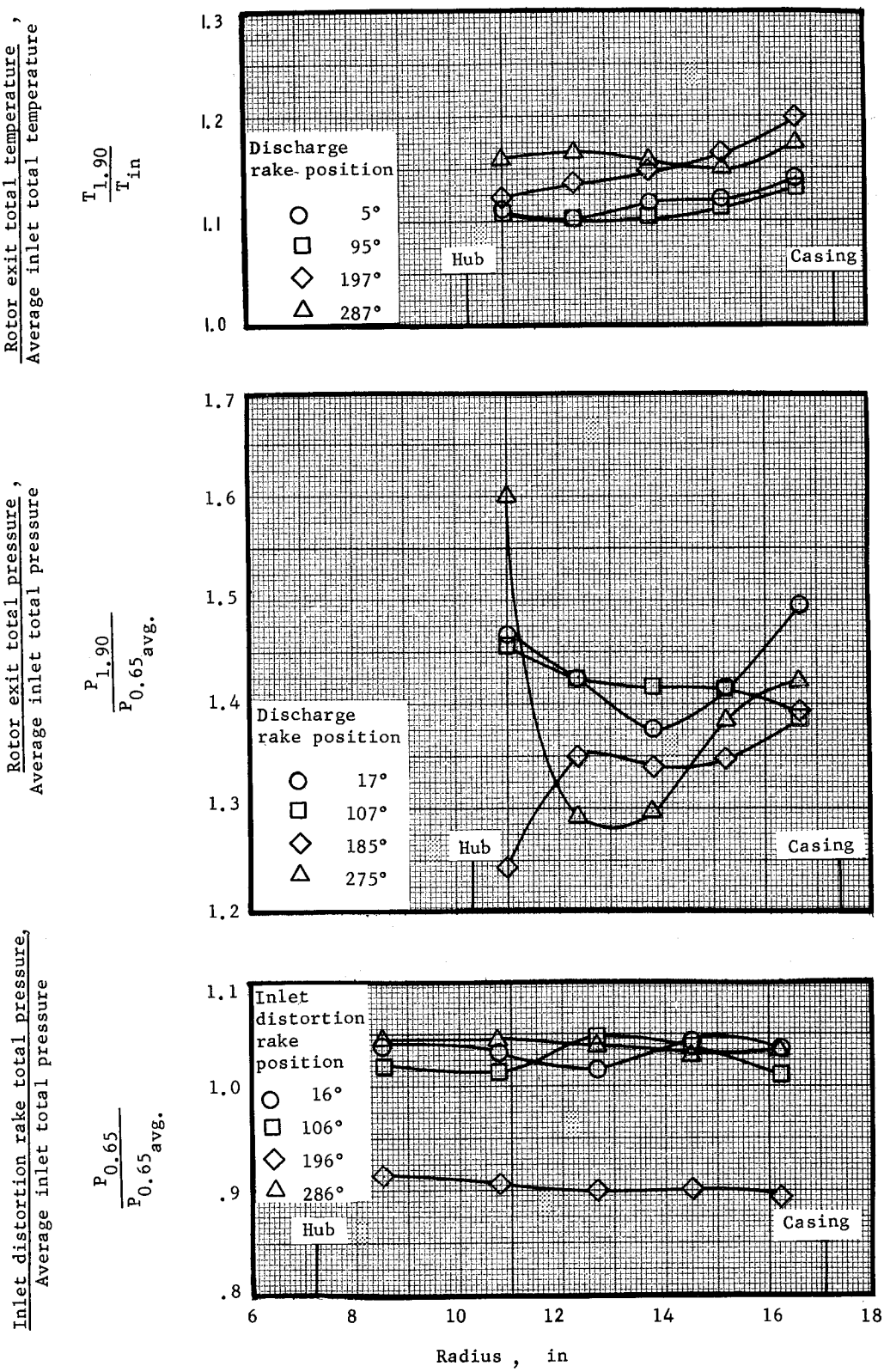

Figure 16 - Inlet total pressure, exit total pressure and exit total temperature profile at 100% design speed, with circumferential distortion, for Reading 86.

DISTRIBUTION LIST

FOR

NASA TASK VI DATA REPORTS

CONTRACT NAS3-7618

1. NASA-Lewis Research Center
   21000 Brookpark Road
   Cleveland, Ohio 44135
   Attention:

Report Control Office	MS 5-5	1
Technical Utilization Office	MS 3-19	1
Library	MS 60-3	2
Fluid System Components Division	MS 5-3	1
Pump and Compressor Branch	MS 5-9	6
A. Ginsburg	MS 5-3	1
M. J. Hartmann	MS 5-9	1
W. A. Benser	MS 5-9	1
D. M. Sandercock	MS 5-9	1
L. J. Herrig	MS 5-9	1
T. F. Gelder	MS 5-9	1
C. L. Ball	MS 5-9	1
L. Reid	MS 5-9	1
J. H. DeFord	MS 77-3	1
S. Lieblein	MS 54-6	1
B. Lubarsky	MS 3-3	1
C. L. Meyer	MS 60-4	1
J. H. Povolny	MS 60-4	1
A. W. Goldstein	MS 7-1	1
J. J. Kramer	MS 7-1	1
W. L. Beede	MS 5-3	1
C. H. Voit	MS 5-3	1
J. H. Childs	MS 60-4	1

2. NASA Scientific and Technical Information Facility
   P. O. Box 33
   College Park, Maryland 20740
   Attention: NASA Representative 6

3. FAA Headquarters
   800 Independence Ave., S.W.
   Washington, D.C. 20553
   Attention: Brig. General J. C. Maxwell 1
   F. B. Howard 1

4. NASA Headquarters
   Washington, D.C. 20546
   Attention: N. F. Rekos (RAP) 1

5. U. S. Army Aviation Material Laboratory
Fort Eustes, Virginia
Attention: John White — 1

6. Headquarters
Wright Patterson Air Force Base, Ohio 45433
Attention: J. L. Wilkins, SESOS — 1
S. Kobelak, APTP — 1
R. P. Carmichael, SESSP — 1

7. Department of Navy
Bureau of Weapons
Washington, D.C. 20525
Attention: Robert Brown, RAPP14 — 1

8. Department of Navy
Bureau of Ships
Washington, D.C. 20360
Attention: G. L. Graves — 1

9. NASA-Langley Research Center
Technical Library
Hampton, Virginia 23365
Attention: Mark R. Nichols — 1
John V. Becker — 1

10. Boeing Company
Commercial Airplane Division
P. O. Box 3991
Seattle, Washington 98124
Attention: C. J. Schott MS80-66 — 1

11. Douglas Aircraft Company — 1
3855 Lakewood Blvd.
Long Beach, California 90801
Attention: J. E. Merriman — 1
Technical Information Center C1-250

12. Pratt and Whitney Aircraft
Florida Research and Development Center
P. O. Box 2691
West Palm Beach, Florida 33402
Attention: R. A. Schmidtke — 1
H. D. Stetson — 1
J. M. Silk — 1
B. A. Jones — 1

13. Pratt and Whitney Aircraft
400 Main Street
East Hartford, Connecticut
Attention: J. A. Fligg — 1
A. W. Stubner — 1
M. J. Keenan — 1

14. Allison Division, GMC
Department 8894, Plant 8
P. O. Box 894
Indianapolis, Indiana 46206
Attention: J. N. Barney — 1
Library — 1

15. Northern Research and Engineering
219 Vassar Street
Cambridge 39, Massachusetts
Attention: R. A. Novak — 1

16. General Electric Company
Flight Propulsion Division
Cincinnati 15, Ohio
Attention: L. H. Smith, H50 — 1
Technical Information Center N32 — 1

17. General Electric Company
1000 Western Ave.
West Lynn, Massachusetts
Attention: L. H. King, Bldg. 2-40 — 1
Dr. C. W. Smith Library Bldg. 2-40M — 1

18. Curtiss-Wright Corporation
Wright Aeronautical
Woodridge, New Jersey
Attention: S. Lombardo — 1

19. Air Research Manufacturing Company
402 South 36th Street
Phoenix, Arizona 85034
Attention: Robert O. Bullock — 1

20. Air Research Manufacturing Company
8951 Sepulveda Boulevard
Los Angeles, California 90009
Attention: Linwood C. Wright — 1

21. Union Carbide Corporation
Nuclear Division
Oak Ridge Gaseous Diffusion Plant
P.O. Box "P"
Oak Ridge, Tennessee 37830
Attention: R. G. Jordan — 1

22. Avco Corporation
Lycoming Division
550 South Main Street
Stratford, Connecticut
Attention: Clause W. Bolton — 1

23. Continental Aviation and Engineering Corp.
12700 Kercheval
Detroit, Michigan 48215
Attention: Eli H. Benstein — 1

24. Solar
San Diego, California 92112
Attention: P. A. Pitt — 1

25. Goodyear Atomic Corporation
Box 628
Piketon, Ohio
Attention: C. O. Langebrake — 1

26. Iowa State University of Science and Technology
Ames, Iowa 50010
Attention: Dept. of Mechanical Engineering — 1

27. Hamilton Standard Division of United Aircraft Corporation
Windsor Locks, Connecticut
Attention: Head of Aerodynamics and Hydrodynamics — 1

28. Westinghouse Electric Corporation
Small Steam and Gas Turbine Engineering B-4
Lester Branch
P. O. Box 9175
Philadelphia, Pennsylvania 19113
Attention: Mr. S. M. DeCorso — 1

29. J. Richard Joy
Supervisor, Analytical Section
Williams Research Corporation
P.O. Box 95
Walled Lake, Michigan — 1

30. Raymond S. Poppe
Building 541, Dept. 80-91
Lockheed Missile and Space Company
P. O. Box 879
Mountain View, California 94040 1

31. James D. Raisbeck
The Boeing Company
224 N. Wilkinson
Dayton, Ohio 45402 1

32. James Furlong
Chrysler Corporation
Research Office
Dept. 9000
P. O. Box 1118
Detroit, Michigan 48231 1

33. Elliott Company
Jeannette, Pennsylvania 15644
Attention: J. Rodger Schields
Director-Engineering 1